MODELING DENITRIFICATION ACROSS AN AGRICULTURAL CATCHMENT IN A CHANGING CLIMATE

A Thesis
Presented to the Faculty of the Graduate School
of Cornell University
In Partial Fulfillment of the Requirements for the Degree of
Master of Science

by
Janet Rice Barclay
August 2013

ABSTRACT

An overabundance of nitrogen (N) in marine and freshwater ecosystems has been linked to diverse, usually negative, effects on human health and the environment. One natural process that reduces N loads to downstream waters is denitrification, the microbially mediated reduction of NO_3^- to N_2, NO, or N_2O gas; however, it is difficult to quantify denitrification rates and even harder to extrapolate them spatially and temporally to generate landscape-scale estimates of denitrification. Additionally, we expect that the changes in temperature and precipitation projected for the end of the century may alter the rates and patterns of denitrification. We developed a coupled hydrologic-denitrification model that predicts daily denitrification rates across an agricultural watershed and was parameterized using *in-situ* denitrification measurements and two types of hydrologic observations (streamflow and upland soil moisture). The model fits well with the observed denitrification (R^2=0.75), stream discharge (R^2=0.71) and soil moisture (R^2=0.85). The modeled values did not match well with areal denitrification observations determined from isotopic analysis of the nitrate and a mixing model, and further work needs to be done to understand this discrepancy. Looking to the future, our results suggest that denitrification rates will increase, particularly in areas with high baseline rates, that the spatial and temporal patterns will not change appreciably, and that temperature increases will be the major driving factor of the projected rate changes.

BIOGRAPHICAL SKETCH

Janet Rice Barclay was born near Cleveland, Ohio on December 15, 1976. She graduated from Hathaway Brown School in 1995 and from The Johns Hopkins University with a Bachelors of Science in Biomedical Engineering in 1999. After graduation, she spent two years assisting undergraduate students in the Department of Biomedical Engineering at Johns Hopkins before spending a year at HoneyRock Camp in Three Lakes, Wisconsin earning a Certificate in Leadership and Camp Ministry. She then moved to New England and spent 8 years working in campus and church ministry with InterVarsity Christian Fellowship and as an associate pastor of a small church. During that time she met and married her husband, Brian Barclay, and they had a son, Ian. While working in campus ministry, Janet became increasingly aware of the many issues affecting water quality, and eventually decided to return to engineering so that she can better assist with environmental restoration.

To Brian and Ian, I love you!

ACKNOWLEDGEMENTS

I would like to thank my committee members – Todd Walter and James Bisogni – for their guidance and support. I would also like to thank the other researchers and faculty who have given me feedback on my project and expanded my understanding through their courses and conversations. Thank you to Todd Anderson for teaching me about denitrification, sharing your data, and passing on your field site. Thank you to the IGERT in Cross-Scale Biogeochemistry and Climate for generous funding and to everyone associated with the IGERT for feedback and encouragement. Thank you to my fellow members of the soil and water lab for their encouragement, feedback, teaching, assistance with field work, and laughter. Thanks to our extended family for your encouragement and for hanging out with Ian while I studied. Finally, thank you to Brian and Ian for your love, encouragement, and support, and for making it possible for me to go to school.

TABLE OF CONTENTS:

LIST OF FIGURES

CHAPTER 1: MODELING DENITRIFICATION

INTRODUCTION

An overabundance of nitrogen (N) in marine and freshwater ecosystems has been linked to diverse, usually negative, effects such as eutrophication and hypoxic dead zones in marine waters, human health issues, marine wildlife mortality, and annual economic losses in excess of $3 billion [1]. The current excess of N results from annual anthropogenic inputs (fertilizer use, agricultural biological fixation and atmospheric deposition) that have doubled since pre-industrial times [2].

One natural process that reduces N loads to downstream waters is denitrification, the microbially mediated reduction of NO_3^- to N_2, NO, or N_2O gas. For example, at the field edge in our study site 60% of the water samples (n=25) exceed the drinking water standard for nitrate of 10 ppm [3]; however by the outlet of the riparian wetland, none of the samples (n=11) exceeded this limit. We speculate that this reduction in nitrate concentration is primarily attributable to riparian denitrification.

Due to the abundance of N in the atmosphere and the complexity of the nitrogen cycle, it is difficult to quantify denitrification rates and even harder to extrapolate them spatially and temporally to generate landscape-scale estimates of denitrification. This type of information is potentially invaluable for developing more effective, targeted management strategies for reducing N-loads to streams and estuaries. Many quantification techniques have been explored, each with advantages and disadvantages [4]. Modeling is a useful tool in the denitrification toolkit because, when correctly calibrated, models can provide estimates of denitrification rates at times and places for which we have no measurements, including the future [5].

Denitrification models vary widely in their approach. Some are highly complex, mechanistic models that attempt to account for the many fluxes, transformations, and pools of N in terrestrial and/or aquatic ecosystems. Others are simpler, collapsing the many rate controlling factors into a few dominate terms. With all models, the level of uncertainty is high due to the difficulty in measuring denitrification rates and the subsequent lack of *in situ* observations [5].

One common simple denitrification model is the reduction function form in which a potential denitrification rate is scaled by multiple reduction function scalars. Each scalar reflects the effects of an individual environmental condition on the denitrification rate. Typically the reduction functions address the effects of temperature, soil moisture, nitrate and occasionally pH. The availability of carbon as a substrate for denitrification is accounted for in the potential denitrification term [6]. We have chosen to use this approach due to the simplicity of calculation and relative ease of gathering the required inputs. Furthermore, increased model complexity does not equate with improved simulation results and can often lead to so many calibration parameters that the model is difficult to constrain, i.e., multiple combinations of calibrated parameters give equally good results [7].

Watershed-scale denitrification models must, at a minimum, simulate both distributed hydrology and denitrification across a landscape because many studies have demonstrated that denitrification is highly sensitive to the soil saturation and related parameters ([6] [8] [9] [10]). However, most hydrologic models primarily utilize stream discharge for calibration. This leaves much uncertainty regarding the ability of the model to accurately predict the heterogeneity of hydrologic conditions throughout the catchment.

Although many techniques exist for calibrating denitrification models, including nitrate flux at the outlet, undisturbed soil cores, *in-situ* soil cores, and N-trace gas fluxes [5] [6] [8] [11], like most hydrology models, most denitrification models are assessed on the basis of their ability to

reproduce observations at the watershed outlet, namely stream-N concentrations . One notable exception is the work of Oehler et al. that utilized the acetylene blockage technique at 15 sites across a small (130 ha) agricultural catchment in France [11]. Acetylene inhibition measurements of denitrification have been widely used due to the ease of taking and analyzing many samples, however the technique has the drawback of potentially underestimating the denitrification rate due to inhibition of nitrification and other biogeochemical effects [4]. The current study applies a similar approach to a larger (1550 ha) agricultural watershed in a cooler (5°C lower mean annual temperature) and wetter climate (37% more rain annually)([11], [12]) and utilizes “push-pull” denitrification measurements which have the advantage of including multiple end-products of denitrification with less disturbance to the system ([13], [14]). Additionally, we have incorporated spatial variation in carbon substrate availability into our model, which was not included in the Oehler study [11], and we have calibrated our hydrologic model with upland observations of soil moisture.

The objectives of this study are 1) to develop a semi-distributed hydrologic model that is tested against hydrologic observations from the outlet and the watershed interior, 2) to utilize field and areal denitrification measurements to parameterize a simple denitrification model for a small agricultural catchment, and 3) to estimate catchment-wide denitrification rates.

MODELS

DENITRIFICATION MODEL

Denitrification is a complex, multi-step reaction process with multiple controlling factors. We choose to focus on the concentration of nitrate, the availability of a carbon substrate, the temperature of the reaction environment, and the extent to which the environment is anaerobic. These factors are relatively easy to measure or model and were found to account for most of the variation in measured denitrification rates.

Though pH has been shown to be a factor in denitrification rate ([6]), we did not consider it in our model due to limited field data. The available pH measurements for the cropped and riparian areas range from 6.5 to 7.9, which is near the optimum of pH 7 [6]. This suggests that pH is probably not a limiting factor in most areas of the catchment. The pH observations from the perched wetland are lower (5.6 and 5.9), which may limit denitrification in this area; however due to low levels of NO_3^- in this area, it does not contribute significantly to watershed-wide rates.

Our denitrification model is a modification of the reduction function format described by Heinen [6], which has the benefit of simplicity and easily measured inputs.

$$D_a = D_{p1}\left(\frac{N}{N+K}\right)\left(Q_{10}^{\left(\frac{T-T_r}{10}\right)}\right)\left(K_c\left(DOC - K_{C1}\right)\right)\left(OM^{(m)}\right)f_s \quad [1]$$

$$f_S = \begin{cases} 0, & S < S_t \\ \left(\frac{S-S_t}{S_m-S_t}\right)^w, & S_t \le S \le S_m \\ 1, & S_m < S \end{cases} \quad [2]$$

Descriptions of the terms of this equation and our parameter values are given in Table 1.

The summary of the models in Heinen ([6]) does not include the *OM* and *DOC* terms. In those models, carbon dynamics are incorporated into the D_p term.

Table 1 – Denitrification Model Terms

Term	Value	Std. Dev.	Description	Units	Source
D_a			Denitrification Rate	kg-N ha^{-1} yr^{--1}	Calculated
D_{p1}	13,233	2752	Potential Denitrification	kg-N ha^{-1} yr^{--1}	Optimization
K	10		Nitrate Rate Constant	ppm NO_3-N	Literature Values [6]
Q_{10}	5.12	1.11	Temperature Constant	Dimensionless	Optimized
T_r	20		Reference Temperature	°C	Literature Values [6]
K_c	1		DOC Unit Conversion	$(ppm\ DOC)^{-1}$	
K_{c1}	.56	0.04	DOC Constant 2	ppm DOC	Optimized
m	1.16	0.09	Soil Organic Matter Exponent	Dimensionless	Optimized
S_t	0.41	.02	Lower Soil Saturation Threshold	Dimensionless	Optimized
S_m	1.0		Upper Soil Saturation Threshold	Dimensionless	Literature Values [6]
w	1.1	0.09	Saturation Function Constant	Dimensionless	Optimized

HYDROLOGIC MODEL

To determine the soil saturation (*S*) that is an input to the denitrification model, we developed a hydrologic model based on the Thornthwaite-Mather available soil water balance [15] and the topographic index concept [16]. Our model tracks the soil water on a daily basis in 10 wetness classes, beginning with the driest class (class 10) and ending with the wettest (class 1) (Figure 1). The wetness classes are equal area, which allows us to track the lateral flows on a depth basis. The calculated variables are defined in Table 2 and the input data and parameters are given in Table 3.

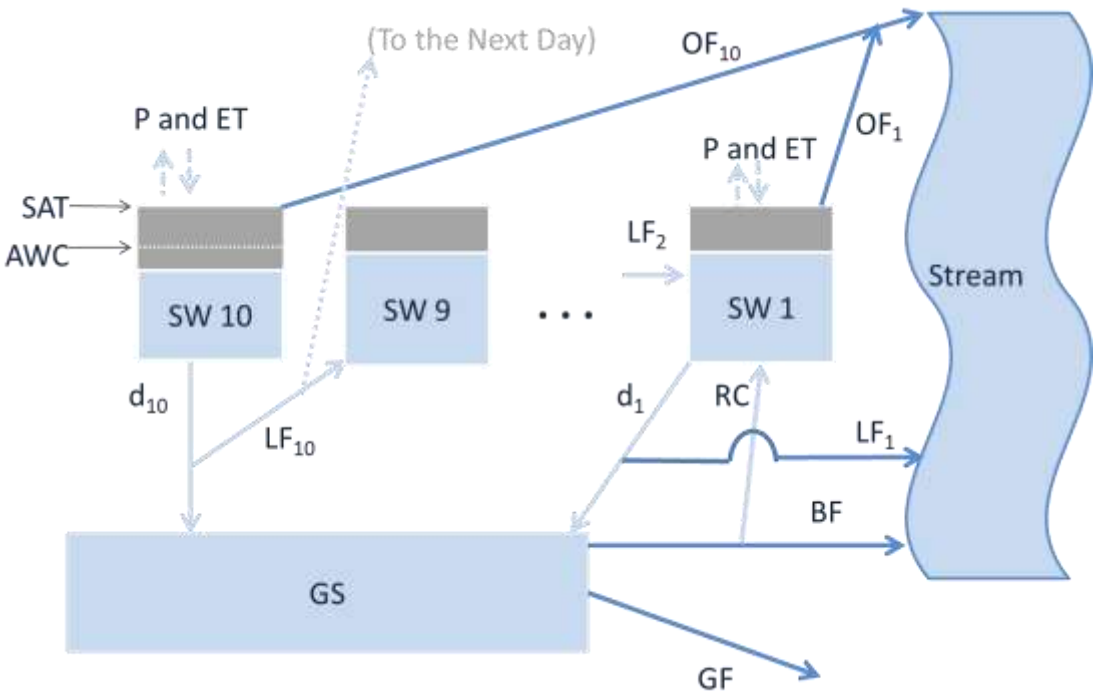

Figure 1 - Hydrologic Model Schematic, showing the major fluxes in the model. Note that not all fluxes are shown for Wetness Class 9 due to space constraints. Variable Descriptions are given in Table 2 and Table 3. Blue boxes indicate water storages, grey boxes indicate soil water deficits, light blue arrows show fluxes among subsurface storages, and dark arrows indicate fluxes to the stream. *P* includes both liquid rain and snowmelt.

Table 2 - Hydrologic Model Calculated Variables

Variable	Units	Description
$\Delta P_{t,i}$	Inches	Net Precipitation on Day *t*, in Wetness Class *i*
PET_i	Inches	Potential Evapotranspiration
M_t	Inches	Snowmelt
$LF_{t,i}$	Inches	Lateral Flow on Day *t* from Wetness Class *i*
$GR_{t,i}$	Inches	Groundwater Recharge on Day *t* from Wetness Class *i*
GS_t	Inches	Groundwater Storage on Day *t*
$d_{t,i}$	Inches	Drainage on Day *t* from Wetness Class *i*
$SW_{t,i}$	Inches	Soil Water on Day *t* in Wetness Class *i*
$OF_{t,i}$	Inches	Overland Flow on Day *t* from Wetness Class *i*
GF_t	CFS	Groundwater Flow on Day *t*
φ_t	Degrees South of West	Angle of Groundwater Flow on Day t
GD_t	Inches-Feet^{-2}	Groundwater Discharge on Day t
RC_t	Inches	Recharge Capacity on Day t
RV_t	Inches-Feet^2	Recharge Volume on Day t
BF_t	CFS	Baseflow
SF_t	CFS	Streamflow
$S_{t,i}$	Dimensionless	Degree of Soil Saturation on Day t in Wetness Class i
$DTW_{t,i}$	Inches	Depth to the Shallow Water Table on Day t in Wetness Class i

Table 3 - Hydrologic Model Input Data and Parameters

Variable	Value	Units	Description	Source
P_t		Inches	Observed Daily Precipitation	[12]
T_{ave}/ T_{min} / T_{max}		°C	Observed Daily Temperature (daily average, minimum, maximum)	[12]
A	168 x10^6	$Feet^2$	Watershed Area	Calculated
A_1	16.8x10^6	$Feet^2$	Area of Wetness Class 1	Calculated
D	19.7	Inches	Depth of the Soil	
η	0.5	Dimensionless	Soil Porosity	[17]
$\Theta_{v,1}$	0.5	Dimensionless	Volumetric Water Content in Partially Saturated Soil in Wetness Class 1	
AWC_1	0.32	Dimensionless	Fraction of soil saturation capacity for the *AWC* in the Wettest Class	Parameterized
AWC	0.40	Dimensionless	Fraction of soil saturation capacity for the *AWC* in all other classes	Parameterized
α	0.71	Dimensionless	Lateralflow Fraction of Daily Drainage	Parameterized
β	0.0082	Dimensionless	Baseflow Fraction of Watershed Storage	Parameterized
δ	0.18	Dimensionless	Fraction of Lateralflow that is delayed 1 day	Parameterized
ε	0.43	Dimensionless	Daily Drainage Fraction of Soil Water above the Available Water Capacity	Parameterized
λ	0.33	Dimensionless	Fraction of Baseflow available for Recharging the wettest soil wetness class	Parameterized
RD	9.3	Inches	Maximum Recharged Depth in Wetness Class 1	Visually Optimized

For each day, the net precipitation in the watershed ($\Delta P_{t,0}$) is calculated:

$$\Delta P_{t,0} = P_t + M_t - PET_t \quad [3]$$

The *PET* is calculated using the Priestly-Taylor equation ([18], [19]) and modified by crop coefficients ([20]). The dates for the crop coefficient milestones were converted to growing degree days (*GDD*) using the annual mean *GDD* from 2005-2011. *The* M_t is calculated on a daily time-step using a process-based snowmelt function ([19]). The Soil Water ($SW_{t,i}$) is

calculated sequentially for each day (*t*) and wetness class (*i*) (driest to wettest) according to the following equations.

Then, the wetness class net precipitation is calculated:

$$\Delta P_{t,i} = \Delta P_{t,0} + LF_{t,i+1} \quad [4]$$

For each class, the $SW_{t,i}$, $d_{t,i}$, and $OF_{t,i}$ are calculated based on $\Delta P_{t,i}$, $SW_{t-1,I}$, AWC or AWC_1, and the Saturation Depth (*SAT*) according to the equations in Table 4.

Table 4 - Flow Chart of Hydrologic Model Terms

$\Delta P_{t,i}$	$SW_{t,i}+\Delta P_{t,i}$		$SW_{t,i}$	$d_{t,i}$	$OF_{t,i}$
$\Delta P_{t,i}>0$ (Wetting Soil)	$SW_{t,i}+\Delta P_{t,i} < AWC_i$ (Non-Draining)	→	$SW_{t-1,i} + \Delta P_{t,i}$	0	0
	$AWC_i < SW_{t,i}+\Delta P_{t,i} <$ SAT (Draining)	→	$SW_{t-1,i} + \Delta P_{t,i} - \varepsilon(SW_{t-1,i} + \Delta P_{t,i} - AWC_i)$	$\varepsilon(SW_{t-1,i} + \Delta P_{t,i} - AWC_i)$	0
	$SW_{t,i}+\Delta P_{t,i} >$ SAT (Saturated)	→	$SAT - \varepsilon(SAT - AWC_i)$	$\varepsilon(SAT - AWC_i)$	$(SW_{t-1,i} + \Delta P_{t,i} - SAT)$
$\Delta P_{t,i}<0$ (Drying Soil)	$SW_{t,i}+\Delta P_{t,i} < AWC_i$ (Non-Draining)	→	$SW_{t-1,i} e^{\frac{\Delta P_{t,i}}{AWC_i}}$	0	0
	$AWC_i < SW_{t,i}+\Delta P_{t,i} <$ SAT (Draining)	→	$SW_{t-1,i} + \Delta P_{t,i} - \varepsilon(SW_{t-1,i} - AWC_i)$	$\varepsilon(SW_{t-1,i} - AWC_i)$	0
	$SW_{t,i}+\Delta P_{t,i} >$ SAT (Saturated)	→	$SAT - \varepsilon(SAT - AWC_i)$	$\varepsilon(SAT - AWC_i)$	$(SW_{t-1,i} + \Delta P_{t,i} - SAT)$

The drainage from each class is split between $LF_{t,i}$ and $GR_{t,i}$ according to the following equations:

$$LF_{t,i} = \alpha\delta d_{t,i} + \alpha(1-\delta)d_{t-1,i} \quad [5]$$

$$GR_{t,i} = (1-\alpha)d_{t,i} \quad [6]$$

GS_i is tracked on a daily timestep:

$$GS_t = GS_{t-1} + \frac{1}{i}\sum_i GR_{t,i} \quad [7]$$

Previous work in this catchment showed that the groundwater gradient (magnitude and direction) varies seasonally as a function of watershed wetness ([21]). We calculated ϕ, the groundwater gradient angle, by the empirical formula:

$$\phi = 114 - 1.4\, SW_{t,2} \quad [8]$$

When φ= 152 degrees South of West the flow is parallel to the stream. Using φ, we calculate the *GF*:

$$GF_t = -10.7 + .117\ \phi \quad [9]$$

The details of these empirical formulas are given in Appendix 1: Groundwater Flow Calculations. The adjusted *GS* is calculated:

$$GS_t = GS_t - GF_t\left(\frac{86400*12}{A}\right) \quad [10]$$

where the factors 86,400 and 12 are units conversions from cfs to inches/day.

GD is calculated according to the following equation:

$$GD_t = \beta GS_t A \quad [11]$$

We assume that the groundwater intercepts the surface soils in the wettest class, allowing the soil water in that class to be recharged according to the following equations:

$$RC_t = \lambda GD_t \frac{1}{A/_i} \quad [12]$$

If the Recharge Capacity is greater than the deficit between the recharge depth and the Soil Water in the wettest wetness class, the Soil Water is fully recharged to the recharge depth.

$$RV_t = \left(RD - SW_{t,1}\right)A_1 \quad [13]$$

$$SW_{t,1} = RD \quad [14]$$

If the Recharge Capacity is less than the deficit between the recharge depth and the Soil Water, the Soil Water is partially recharged.

$$RV_t = (RC_t)A_1 \quad [15]$$

$$SW_{t,1} = SW_{t,1} + RC_t \quad [16]$$

If the Soil Water is greater than the recharge depth, no recharge occurs and the recharge volume is 0.

Baseflow is the groundwater contribution to the streamflow:

$$BF_t = (GD_t - RV_t)\left(\frac{1}{12*86400}\right) \quad [17]$$

The factors 12 and 86400 convert from inches to feet and days to seconds, respectively.

SF is the combination of BF_t, $OF_{t,i}$ and $LF_{t,1}$ from the wettest class.

$$SF_t = BF_t + \left(LF_{t,1} + \frac{1}{10}\sum_i OF_{t,i}\right)\left(\frac{A}{12*86400}\right) \quad [18]$$

The factors 12 and 86400 convert from inches to feet and days to seconds, respectively, and the factor (1/10) averages the overland flow across the 10 wetness classes.

$S_{t,i}$ is calculated:

$$S_{t,i} = \frac{SW_{t,i}}{SAT} \quad [19]$$

DTW in Class 1 is calculated by:

$$DTW_{t,1} = \frac{D\eta - SW_{t,1}}{(1-\theta_{v,1})\eta} \quad [20]$$

We used a constant porosity of 50% ([17]) and a soil depth of 50 cm.

The wetness classes are mapped onto the watershed using the Soil Topographic Index (*STI*) ([16]):

$$STI = \ln\left(\frac{a}{D\,K_{sat}\tan\beta}\right) \quad [21]$$

where *a* = the upslope contributing area per unit length of contour, *D* is the soil depth (cm), K_{sat} is the saturated hydraulic conductivity (μm/s), and *β*= the topographic slope (radians). The resulting *STI* values were grouped into 10 quantiles, with the highest values corresponding to wetness class 1 (the wettest wetness class) and the lowest values to wetness class 10 (the driest wetness class) (Figure 2A).

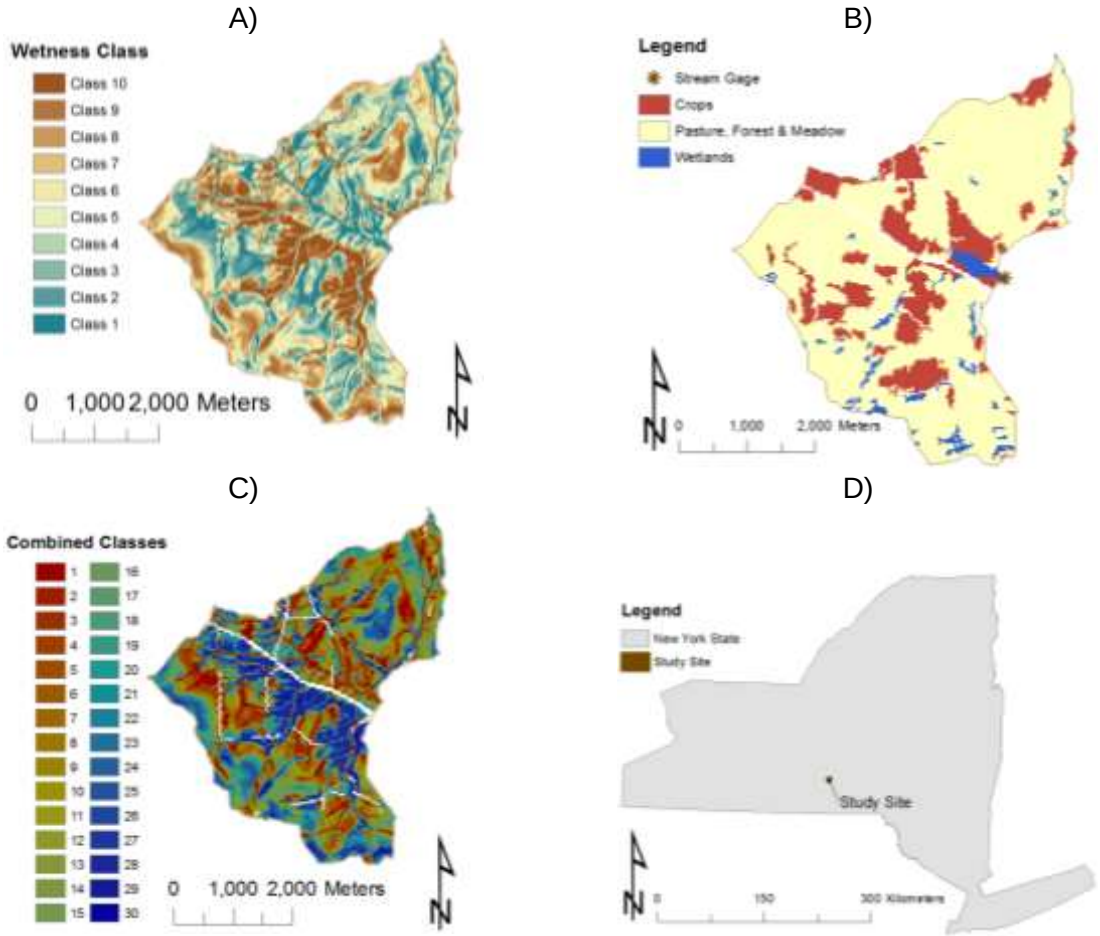

Figure 2 – Maps of the Study Watershed: A) The Soil Topographic Indexed, binned by quantile into 10 equal area wetness classes; B) The Primary Land Uses in the Catchment; C) The 30 Unique Combinations of Wetness Class and Land Use which formed the calculation basis for the denitrification model; D) The Watershed's location within the Finger Lake region of New York State

TEMPERATURE MODEL

Soil temperature was modeled according to the STICS equation used in TNT2 ([22], [23], as referenced in [11]):

$$T_{soil_t} = T_{soil_{t-1}} + a\left(T_{air_{t-1}} - T_{soil_{t-1}}\right) + e^{-8.23*z_{soil}}\left(T_{air_t} - T_{air_{t-1}}\right) \quad [22]$$

Where T_{soil} is the soil temperature (°C), T_{air} is the air temperature at the ground surface (°C), subscripts *t* and *t-1* denote the current and previous days, respectively, and z_{soil} is the soil depth (m). In the wettest *STI* class where we assume that groundwater influences the soil temperature, the modeled soil temperature is averaged with the annual average soil temperature to simulate this effect.

SITE DESCRIPTION

We applied our model to the southern watershed draining the Cornell University Teaching and Research Farm in Harford, NY (Figure 2D). The elevation in this 1550 ha watershed ranges from 360 to 613 m. The northeastern and southwestern highlands drain to a central floodplain, which empties to the southeast into the East Branch of Owego Creek, and then into the Upper Susquehanna River. In the central valley bottom, the primary soil type is Howard gravelly loam and on the adjacent hillslopes the primary soil types are Langford channery silt loam and Volusia channery silt loam [24]. The watershed is at the intersection of Tompkins, Tioga and Cortland Counties and the primary land uses are forest and agriculture (Figure 2). The primary N input to the soil in this watershed is through manure fertilizer. The organic N and ammonium in the manure are readily converted to NO_3^- through ammonification and nitrification.

The spatial and temporal distribution of DOC and NO_3-N were modeled based on land use. NO_3-N in the cropped areas and wetlands were assumed to be constant at 4.7 ppm and 7 ppm, respectively based on field observations (data not shown), a dataset from Bouldin [25], and field observations from Dahlke [26]. NO_3-N in the forest and pasture areas ranges according to a

sinusoidal function of the Julian Day from 0.05 and 0.55 ppm. DOC was assumed to be constant in cropped (3.1 ppm), and in forests/pastures (4.7 ppm). DOC in the wetlands varied according to a seasonal step function, with a value of 5.7 ppm in the summer (175 < Jday < 310) and 1.45 ppm the rest of the year. These DOC estimates are based on 127 direct measurements (data not shown). When the hydrologic wetness classes are overlaid with the three primary land uses, 30 distinct classes result (Figure 2C). Denitrification rates are calculated on a daily basis for each class.

Soil organic matter levels throughout the watershed were modeled based on land use and *Wetness Class*. In wetlands of the wettest class, the SOM is taken to be 22.4% and in all other areas of the watershed the SOM is assumed to be 8.0%. These values are based on 17 direct measurements and are higher than the values reported in the USDA soil survey [24].

METHODS

HYDROLOGIC MODEL PARAMETERIZATION

The hydrologic model was compared against the stream discharge at the watershed outlet and the soil moisture at the weather station and the parameters were optimized (Table 3) to obtain the highest Nash-Sutcliffe efficiency (NSE) [27] for these observations. The NSE for the stream discharge and the NSE for the NSE for the soil moisture were averaged in the parameterization process. The NSE is calculated

$$\mathrm{NSE} = 1 - \frac{\Sigma(Q_{obs} - Q_{mod})^2}{\Sigma(Q_{obs} - \overline{Q_{mod}})^2} \quad [23]$$

Where Q_{obs} is the observed value and Q_{mod} is the modeled value. The NSE ranges from -∞ to 1, with 1 indicating a perfect match with the observations and negative numbers indicating a worse match than the mean observation [27]. The optimization was done using the DEoptim package in R [28]. The parameters were optimized using the 2009-2011 data and the model was corroborated using the 2012-2013 data. After parameterization, we visually compared the

modeled and observed water table depth in the wettest class; the water table depth data were too sporadic to meaningfully test the model.

Weather Data (temperature, precipitation, soil temp, soil moisture)

Climate data (temperature, precipitation) for the watershed were downloaded from the onsite NOAA weather station (NY Ithaca 13E) [12]. This data set also included soil temperature and soil moisture at the weather station, which we downloaded for testing model predictions. The data were obtained in hourly increments and aggregated by day prior to use in the model. Due to the small size of the watershed, we assumed the air temperature and precipitation were uniform across the study site.

Stream Gage

To compare the modeled and observed discharge, we measured streamflow at the watershed outlet (Figure 2B) during two time periods (July 2009 – August 2010 and June 2012-May 2013); the gap in measurements corresponds to a period when we were not involved with field research at this site. During each time series, stream depth was measured at 10 minute intervals with an Odyssey Capacitance Water Level Logger. The stream stage was converted to discharge rates with a rating curve that was generated by correlating stage against periodic wading-rod stream discharge measurements ([29]) using a Marsh-McBirney Flo-Mate Model 2000 portable flowmeter. During the first time period, we made 23 wading-rod measurements ranging from a depth of 38 cm (1.46 cfs) to 49 cm (6.94 cfs); in the second period we made 13 measurements ranging from a depth of 29 cm (0.13 cfs) to 56 cm (10.92 cfs).

Soil Temperature Model Parameterization

To better fit our observed soil temperature values, we adjusted the *a* parameter in the Soil Temperature Model to maximize the R^2 value and minimize the Root Mean Square Error

(RMSE). We used the soil temperature at a depth of 50cm and found the best fit with *a*=.08, which is slightly smaller than the original model.

CLASS 1 SOIL TEMPERATURE

We assumed the soil temperature was equivalent to the groundwater temperature of the same depth. Soil temperature in wetness class 1 was measured with Odyssey Depth/Temperature logger at two locations at 10 minute intervals over a period of 10 months (June 2012 – May 2013)

PUSH-PULLS

The denitrification model was parameterized using 94 *in-situ* "push-pull" measurements made over two years at three landscape positions ([13], [14]). In this method, ^{15}N labeled NO_3^- is injected into shallow (50 cm) groundwater wells. After an incubation period, water samples are withdrawn and injected into evacuated glass bottles. After a second incubation period, the gases in the headspace of the bottles are analyzed to quantify the denitrification rate. The details of these measurements and data points are given in Anderson [30].

The push-pull measurements were taken in the saturated zone; therefore, we multiplied the measured value by z_{eff}, an effective depth based on the amount of soil organic matter in the saturated zone of the soil:

$$C(z) = C_0 e^{-nz} \quad [24]$$

$$z_{eff} = z_{tot} \frac{\int_z^{z_{tot}} C(z)dz}{\int_0^{z_{tot}} C(z)\,dz} \quad [25]$$

Where z is the depth in the soil (cm), z_{tot} is the well depth (50 cm), $C(z)$ is the soil organic matter percent at depth z, C_0 is the soil organic matter percent at the surface (z=0) and n is a coefficient of soil organic matter depletion with depth. Values for C_0 and n were determined experimentally (data not shown).

Denitrification Model Parameterization

We performed a “leave-one-out” optimization process in which one data point is removed from the dataset, the remaining data are used to optimize the parameters such that the RMSE is minimized, and then the optimized parameters are used to calculate the residual for the removed data point. This process is repeated for each data point, and then the mean optimized value for each parameter is selected. We performed this optimization using the DEOptim package in R [28].

Soil Organic Matter

Soil cores (7 cm diameter) were taken of the top 7 cm in 15 locations in riparian areas and along the field edge. Samples were oven dried at 105°C for 48 hours. Subsamples were burned for 4 hours in a muffle furnace at 550°C to calculate the percent of organic matter. Organic matter was assumed to be 50% of the loss on ignition ([31]).

Sensitivity Analysis

Sobol Indices [32] were used for the sensitivity analysis of the denitrification and hydrologic models. Sobol Indices are a variance based sensitivity analysis method that breaks the variance into components associated with each parameter. The power of the Sobol Indices is that it allows the interactions among parameters to be considered, unlike one-at-a-time sensitivity analysis methods. The Indices were calculated using the Sensitivity Package in R [33] with parameters order=3, and nboot=100. For the denitrification model, we used n=50,000, and for the hydrologic model we used n=10,000 due to increased computational cost in running the hydrologic model.

RESULTS

PUSH-PULL COMPARISONS

We used 94 *in-situ* "push-pull" denitrification measurements to parameterize our denitrification model (Figure 3 and Table 1). With the exception of the depth to the water table used in calculating z_{eff} for 23 data points, the parameterization was performed independently of the hydrological model. Parameter optimization was done using the DEoptim package in R [28].

After parameterization, the residual factor appeared to have a seasonal trend, so we incorporated a sinusoidal function and re-optimized the parameters (Table 1). The final denitrification function takes the form:

$$D_a = D_{p1}\left(\frac{N}{N+K}\right)\left(Q_{10}^{\left(\frac{T-T_r}{10}\right)}\right)\left(K_c(DOC - K_{C1})\right)(OM^m)f_s\left(sin\left(\frac{2\pi}{365}(Jday - J_0)\right) + D_{p-Offset}\right) \quad [26]$$

Where *Jday* is the Julian day of the year, J_0 is a date offset, and $D_{p\text{-}offset}$ is an offset to the sinusoidal function. The optimized value for $D_{p\text{-}offset}$ is 1.05 ±0.04 and for J_0 is -3.55 ±7.04 Days. The parameterized model fits well with the measured values. (R^2= 0.77, n=94, RMSE=272 kg-N ha^{-1} yr^{-1}). When the data are aggregated by month (R^2= 0.93) or by well (R^2= 0.80), the model agreement is even better.

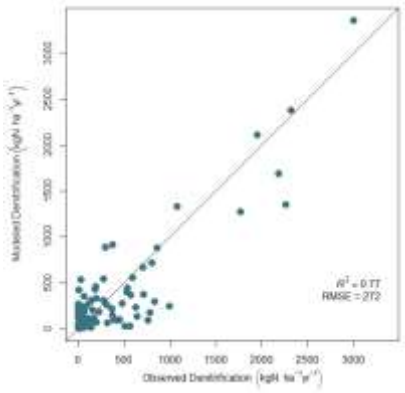

Figure 3 – Model Comparison to *In-Situ* Push-Pull Denitrification Measurements

HYDROLOGIC MODEL

We assessed the hydrologic model with two sets of hydrologic observations: 1) streamflow at the watershed outlet, and 2) soil moisture (10 cm depth) at the weather station (Figure 4). Observations from 2009-2011 were used to parameterize the model and observations from 2012-2013 were used to assess the model performance. With both datasets we used the Nash-Sutcliffe efficiency (NSE) [27] to evaluate the streamflow and soil moisture simulations. During the parameterization period, the NSE for the streamflow is 0.88 and for the soil moisture is 0.87; for daily stream discharge an NSE of 0.87 is considered very good ([34]). During the verification period, the NSE for the streamflow is 0.55 and for the soil moisture is 0.84; for daily stream discharge an NSE of 0.55 is good ([34]). For the combined datasets, the discharge NSE is 0.71 and the Soil Moisture NSE is 0.85. We also compared the modeled and observed depth to the water table in the riparian area and the model captures the seasonal trends satisfactorily (data not shown).

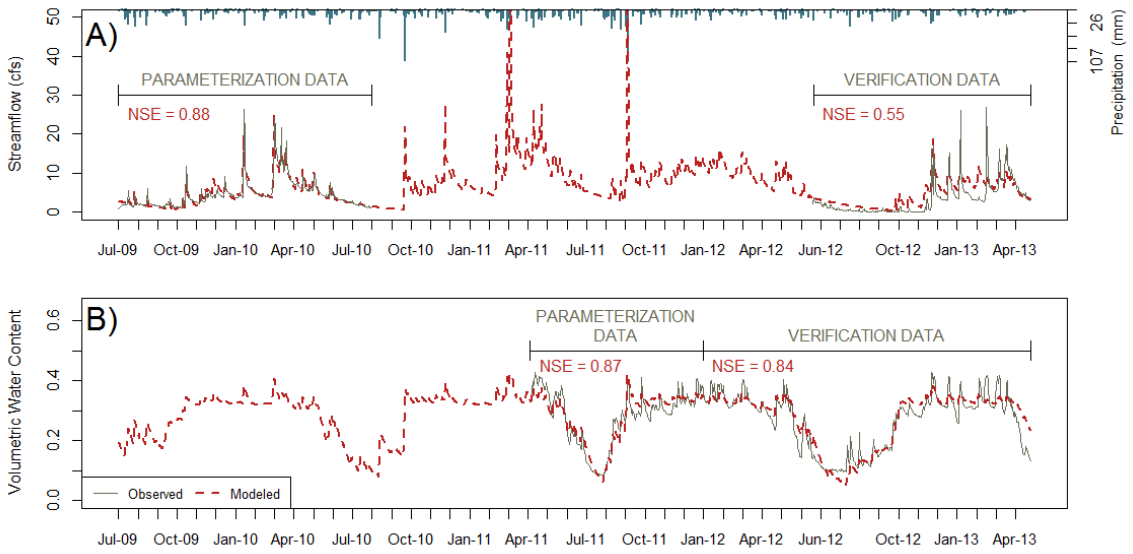

Figure 4 - Hydrologic Model Comparisons: A) Comparison of Modeled and Observed Stream Discharge, B) Comparison of Modeled and Observed Soil Moisture in an Upland Area. Dashed red lines = model, solid grey line = observations. Precipitation is shown as inverted bars in (A).

SOIL TEMP

We compared our soil temperature model with the measured soil temperature at 50 cm depth from the weather station (upland) and with the observed groundwater temperature at 50 cm depth in two wetlands (Figure 5). Both the upland and wetland models fit the observed temperatures well, with R^2 values of 0.98 and 0.84 and RMSE values of 2.25 ^{o}C and 3.12 ^{o}C, respectively. The largest deviations were in the winter when the model systematically over-estimated soil temperature. This is typically not a period associated with high denitrification rates.

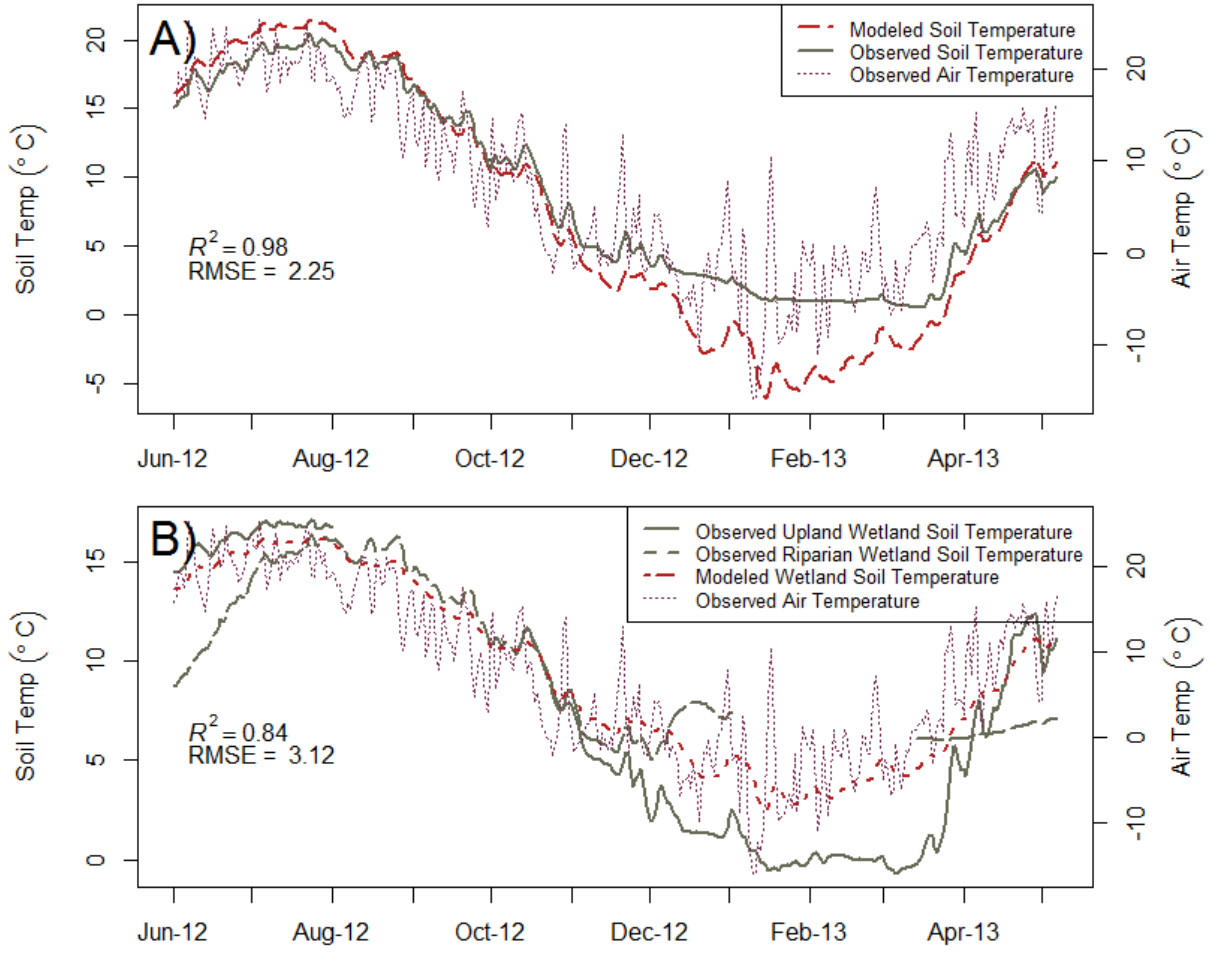

Figure 5 - Temperature Model Results – A) The comparison of the modeled and observed upland soil temperature; B) The comparison of the modeled and observed wetland soil temperature – The observed wetland temperatures are from two wetlands, one in the riparian area and one perched on the hillside.

WATERSHED-WIDE DENITRIFICATION RATES

The mean modeled annual denitrification rates for various areas of the watershed are given in Table 5.Modeled average annual denitrification rates are shown in Figure 6, and the modeled seasonal rates are shown in Figure 7. As expected, the highest annual rates occur primarily in the wetlands between the cropped fields and the stream. The highest rates typically occur in late May and June, after the soil has warmed and before it dries significantly.

SENSITIVITY ANALYSIS

The Sensitivity Analysis indicates that within the bounds of the standard deviation from the parameter optimization, the denitrification model is most sensitivity to m and Q_{10} (Figure 8A). If the parameters are allowed to vary within the greater range seen in the literature ([6], [35]), the model is most sensitive to the S_t, with lesser sensitivities to w and Q_{10} (Figure 8B). On the input side, the model is most sensitive to the inputs of *OM* and *SoilSat* (Figure 8C). The hydrologic model is most sensitive to the parameter for the available water capacity, *AWC* (Figure 8D).

Table 5- Mean Annual Modeled Denitrification Rates

Area	Mean Annual Rate
Watershed	9.6 kg-N ha^{-1} yr^{-1}
Wetness Class 1	35.7 kg-N ha^{-1} yr^{-1}
Wetlands in Wetness Class 1	200.8 kg-N ha^{-1} yr^{-1}
Wetlands	46.5 kg-N ha^{-1} yr^{-1}
Cropped Areas	30.3 kg-N ha^{-1} yr^{-1}
Forests, Pastures, & Meadows	2.3 kg-N ha^{-1} yr^{-1}

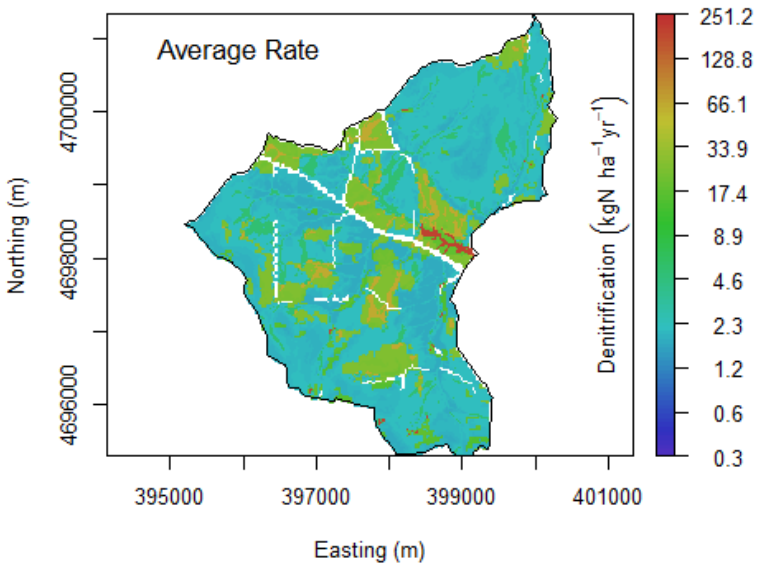

Figure 6 - Watershed-wide Denitrification Rates – (modeled annual averages from 2005-2011)

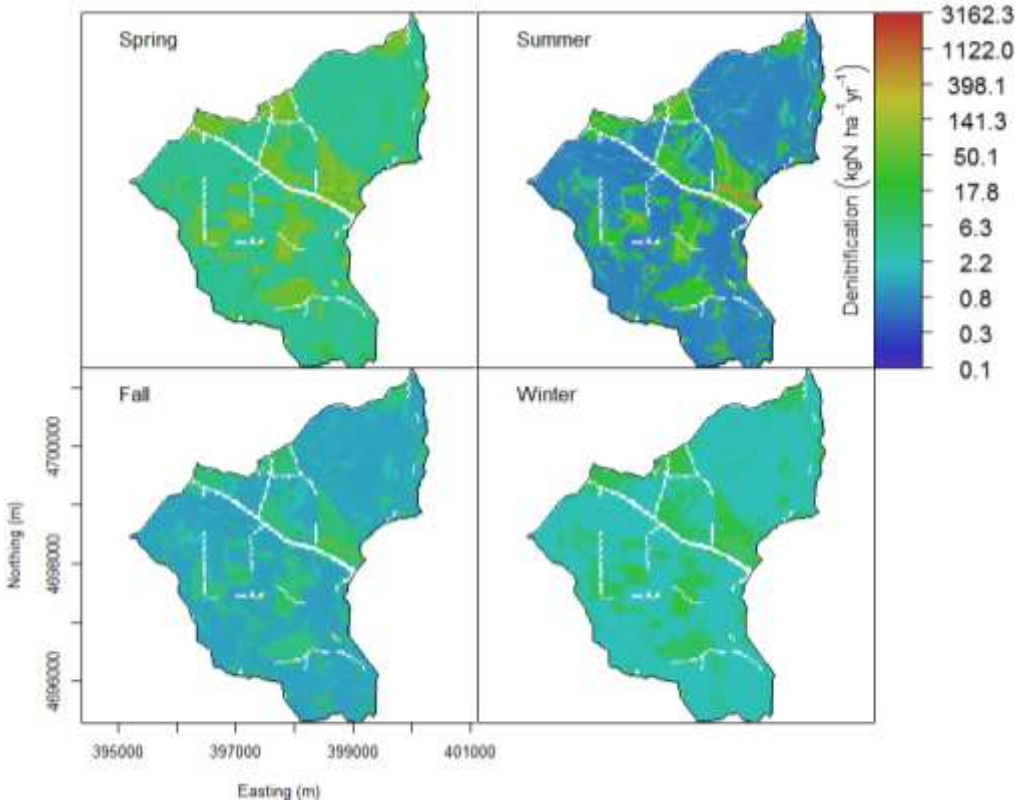

Figure 7 - Seasonal Denitrification Rates - These rates are the modeled seasonal averages from 2005-2011. Spring rates are from March – May, Summer rates are from June – August, Fall rates are from September – November, and Winter rates are from December – February.

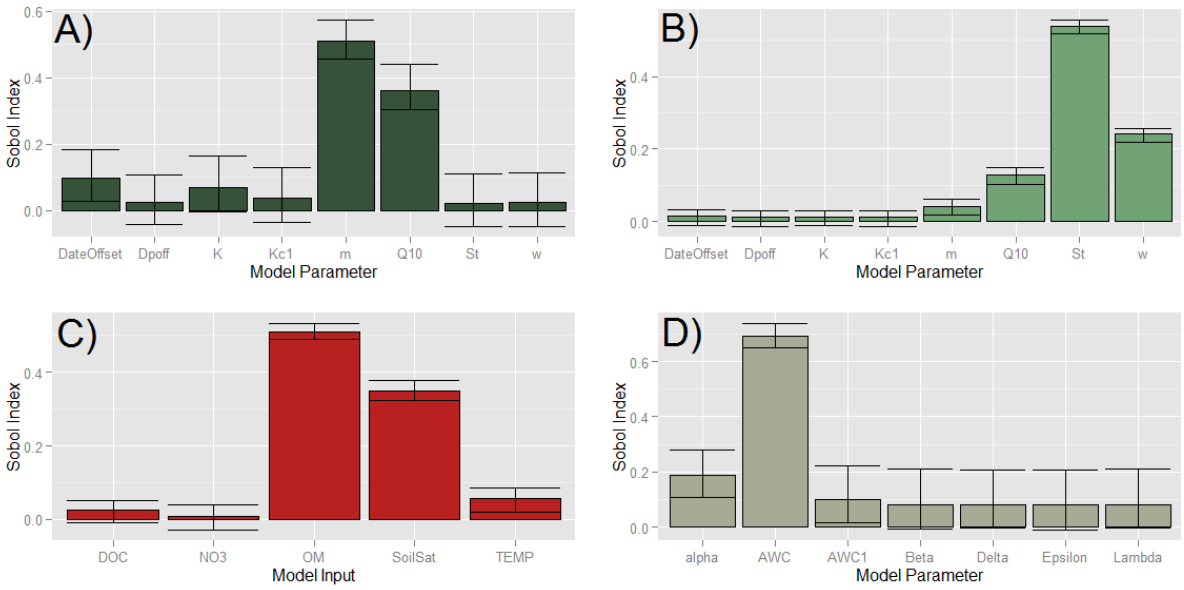

Figure 8 - Sensitivity Analysis Results – A) Denitrification Model Parameters with variances within the standard deviation from optimization results; B) Denitrification Model Parameters with variances within the range of literature values; C) Denitrification Model Inputs; D) Hydrology Model Parameters

DISCUSSION

SINUSOIDAL FUNCTION

After our initial parameter optimization of the denitrification model, we observed a slight seasonal pattern in the ratio of observed and modeled values. To account for this seasonal trend in the observed rates, we added a sinusoidal function to the model, which decreased the RMSE from 328 to 258. (R^2 increased from 0.67 to 0.79) This sinusoidal function peaks in late March (*Jday*=87) and reaches a low value in August (*Jday*=268). This is consistent with observations by Hénault and Germon that potential denitrification rates drop significantly in the summer season [8]. The physical basis for this decline may be a shift the in quality of the available carbon.

PARAMETERIZATION OF THE HYDROLOGIC AND DENITRIFICATION MODELS

We successfully parameterized both the denitrification and hydrologic model for this agricultural watershed. The denitrification model matches well the *in-situ* push-pull measurements and the

optimized parameters are well within the ranges seen in the literature (Table 6), with the exception of *m* and K_{c1}, for which we have not seen values reported. Our values for D_p vary more broadly than the literature values because we have incorporated spatially and temporal components of the carbon dynamics.

Table 6 – Denitrification Parameter Comparison with Literature Values

Term	Our Value(s)	Description	Units	Heinen [6]	Heinen [35]	Oehler et al [11]
D_p	88 – 14,000	Potential Denitrification	kg-N ha^{-1} yr^{-1}	-	978-14,052	4621-7269
Q_{10}	5.12	Temperature Constant	Dimensionless	2-3	2.44-10	2
S_t	0.41	Lower Soil Saturation Threshold	Dimensionless	0.5 – 0.9	0-0.83	19.5
w	1.1	Saturation Function Constant	Dimensionless	0-2.5	1-15.09	1.27

If the variance in the denitrification model parameters is within the standard error range of our parameterization, the model is most sensitive to errors in *m* and Q_{10}, however, if the parameters vary more broadly within the range reported by Heinen ([35], [6]), the model is most sensitive to errors in S_t, with somewhat lesser sensitivities to *w*, and Q_{10}. On the input side, the model is most sensitive to errors in the inputs of *OM* and *SoilSat*. Others have noted that denitrification models are typically most sensitive to the parameters and inputs of the soil saturation reduction function ([6], [9], [4], [8]). Since the carbon dynamics of most simple denitrification models are incorporated into *Dp*, our terms *OM* and *m* are not included in other published sensitivity analyses. With this consideration, our input sensitivity analysis and the broader parameter sensitivity analysis fit well with what others have seen. Due to the significance of carbon availability to denitrification and the structure of our model, it is not surprising that *OM* and *m* are important values. The sensitivity of the model to the value of Q_{10} is surprising, since Heinen found that a simple denitrification model similar to ours was relatively insensitive to variances in the temperature related values ([6]).

COMPARISON WITH *IN-SITU* MEASUREMENTS

Because our model has been successfully compared with *in-situ* denitrification measurements and multiple sets of hydrologic observations, we have greater confidence in the ability of our model to accurately represent the spatial and temporal variation throughout the watershed. This is critical since research has shown that the bulk of denitrification occurs in "hot spots" and "hot moments." ([10], [36], [37]) To accurately estimate denitrification rates in these hot spots and during hot moments, we must accurately represent the spatial and temporal variation in the factors affecting denitrification rates. The rates in **Error! Reference source not found.** compare reasonably well with the rates calculated by Oehler et al. (47.0 kg-N ha^{-1} yr^{-1} watershed-wide, 92.6 kg-N ha^{-1} yr^{-1} in the riparian areas and 34.5 kg-N ha^{-1} yr^{-1} in the hillslopes) [11], and with Ferrant et al. (26 kg-N ha^{-1} yr^{-1} with TNT2 and 25 kg-N ha^{-1} yr^{-1} with SWAT) [38]. Both of these studies used watersheds with a higher percentage of cropped land (85% and 60% respectively, compared to 20% in our watershed). The rate is well below the estimate of Van Breeman et al of 62 kg-N ha^{-1} yr^{-1} for the entire Susquehanna River Basin which was based on the difference between estimated inputs and known output of nitrogen [2].

CONCLUSIONS

We developed a coupled hydrologic-denitrification model that predicts daily denitrification rates across an agricultural watershed. A unique feature of this model is that the denitrification module was parameterized using *in-situ* measurements, and the hydrologic module was parameterized using two types of hydrologic observations (streamflow and upland soil moisture). This enhances our model's ability to predict denitrification rates at the full range of environmental conditions. In the future, this model will allow us to further examine the spatial and temporal patterns of denitrification, particularly in a changing climate.

CHAPTER 2: DENITRIFICATION ESTIMATES USING NATURAL ABUNDANCE ISOTOPES OF ^{15}N AND ^{18}O

INTRODUCTION

Isotopes of ^{15}N and ^{18}O are commonly used to disentangle the many processes that transform nitrate ([4], [39], [40], [41]). The isotopic composition of the nitrate is analyzed to determine $\delta^{15}N$ and $\delta^{18}O$, the ratio of the ratio of heavy to light isotopes in the sample compared to a standard, which are calculated as follows [40]:

$$\delta^{15}N = \left(\frac{{}^{15}N_{sample} / {}^{14}N_{sample}}{{}^{15}N_{standard} / {}^{14}N_{standard}} - 1 \right) * 1000 \qquad [27]$$

To calculate $\delta^{18}O$ from the above equation, ^{15}N is replaced by ^{18}O and ^{14}N is replaced by ^{16}O. For nitrogen the standard is atmospheric N_2 and for oxygen the standard is Vienna Standard Mean Ocean Water [40].

Denitrification has been shown to fractionate against the heavier isotopes of O and N, therefore along a flow path, the indications of denitrification include 1) decreasing nitrate concentration, 2) increasing $\delta^{15}N$, 3) increasing $\delta^{18}O$, and 4) a $\delta^{18}O$: $\delta^{15}N$ slope of 0.5 to 1 ([39], [4], [40]). We analyzed the isotopic composition of groundwater and stream water in the Riparian Area (Figure 9) to calculate an Areal denitrification rate. As shown in Figure 11, in the Riparian Area, from the edge of the field to the points within the riparian area, NO_3-N decreases and both $\delta^{18}O$ and $\delta^{15}N$ increase with a slope of 0.74 ($\delta^{18}O$ ‰ / $\delta^{15}N$ ‰), which is consistent with denitrification being a primary transformative process in this area. We calculated the areal denitrification rate using a mixing model and mass balance approach with chloride as a conservative tracer. [39]

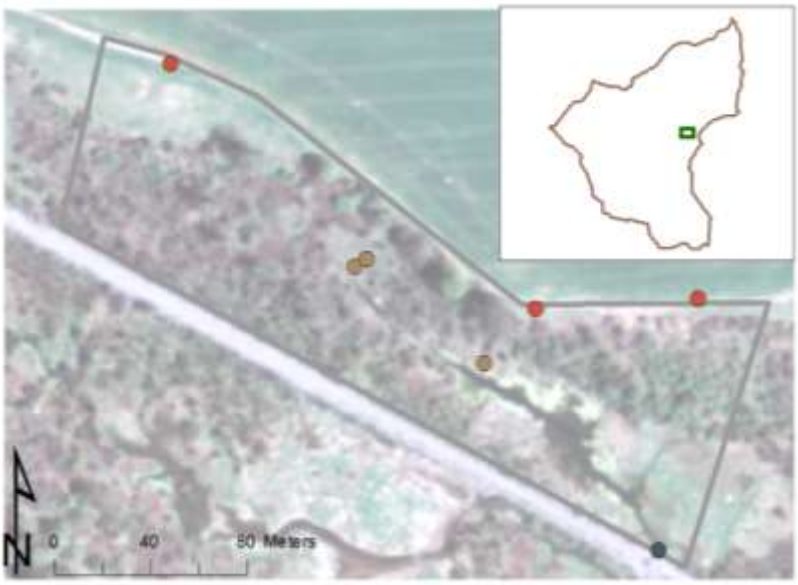

Figure 9 - Riparian Area: Red Circles mark the Field Edge Wells, Brown Circles mark the Riparian Area Wells, and the Blue Circle makes the Culvert where the Riparian Area empties into the stream

METHODS

WATER SAMPLES

Groundwater samples were collected from existing wells using a MasterFlex E/S Portable Sampler peristaltic pump. Streamwater samples were collected at mid-depth using a 1 L bottle. Water temperature and dissolved oxygen content were measured in subsamples, and the remaining water sample was filtered through a 0.2 μm filter when field conditions permitted. When field filtering was not practical, samples were filtered within 6 hours. Water samples were transported on ice to the laboratory where they were refrigerated up to 24 hours prior to analysis for NO_3-N, chloride (Cl), and DOC and then frozen.

Aqueous NO_3-N and Cl were measured using a Dionex ICS-2000 Ion Chromatograph. Dissolved organic carbon was measured using an O-I Analyzer 1010 Total Organic Carbon Analyzer. Frozen water samples were shipped to the UC Davis Stable Isotope Facility where analysis for ^{15}N and ^{18}O in the NO_3^- (aq) was performed according to the bacterial denitrification method. [42] [43]

CULVERT DISCHARGE

The discharge from the culvert at the outlet of the Riparian Area (Figure 9) was used in the calculation of isotopic estimates of riparian denitrification. We measured the stream discharge at the outlet culvert on seven occasions between July and October of 2012 using the wading-rod method that was used for stream discharge.

FIELD EDGE ESTIMATES

We calculated the average Cl^- and NO_3^- concentrations at the field edge of the riparian area based on measurements from three shallow groundwater wells (Figure 10, n=12). We fit the data points to a curve of the form

$$y = a + e^{bx} \quad [28]$$

where *y* is the concentration (ppm), *x* is the distance along the field edge (m), and a & b are fitted coefficients, and found the average concentration along the field edge for each sampling day. For days with only one available data point (n=6), we used the average from the other points for *a* and calculated *b*.

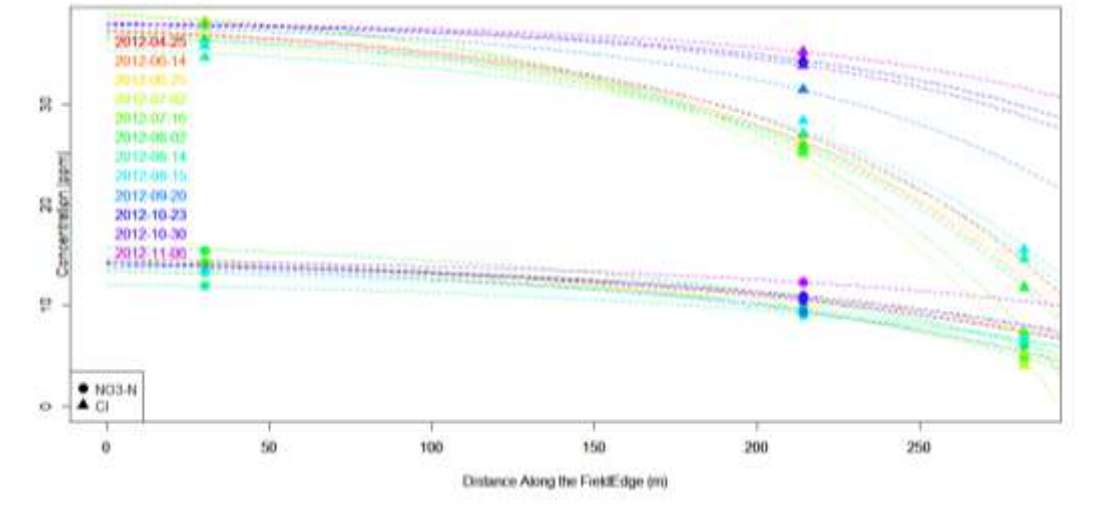

Figure 10 - Chloride (triangles) and Nitrate (circles) Concentrations along the Field Edge of the Riparian Area (Figure 9)

DENITRIFICATION MEASUREMENTS FROM ISOTOPES AND MASS BALANCES

Based on the relationship between $\delta^{15}N$ and $\delta^{18}O$ (Figure 11), we concluded that denitrification is a primary process contributing to the loss of nitrate in the riparian area and calculated the areal denitrification rate using a mixing model and mass balance approach with chloride as a conservative tracer.

We modeled the flux through the culvert outflow of riparian area as a mixture of groundwater baseflow, surface / lateral flow through the riparian area, and rainwater.

$$[Cl]_1 Q_1 = [Cl]_2 Q_2 + [Cl]_3 Q_3 + [Cl]_4 Q_4 \quad [29]$$

$$Q_1 = Q_2 + Q_3 + Q_4 \quad [30]$$

$$[NO_3 - N]_1 Q_1 + \frac{D}{A} = [NO_3 - N]_2 Q_2 + [NO_3 - N]_3 Q_3 + [NO_3 - N]_4 Q_4 \quad [31]$$

[Cl] and [NO_3-N] are the concentrations of Chloride and Nitrate (ppm) respectively, Q is the volumetric water flow (cfs) and the subscripts 1-4 denote the riparian area outlet, baseflow, surface / lateral flow into the riparian area, and rain flow, respectively. *D* is the denitrification rate and *A* is the area of riparian area A. We assume the system is at steady-state with regards to the water and chloride.

We assumed the groundwater composition was constant at 22.8 ppm Cl and ppm NO_3-N, which we took from the outlet composition in the late fall when we assumed that baseflow was the primary component. When the preceding 24 hr precipitation total was greater than 3 cm, 20% of the rainfall to the riparian area was included. Rainfall composition was assumed to be constant at 0.07 ppm Cl and 0.23 ppm NO_3-N based on annual measurements of wet deposition from Connecticut Hill, Newfield, New York (approximately 35 km west of the study site) and the annual rainfall average ([44]).

Using the above equations, we solved for Q_2 and Q_3, and then used these values to calculate *D*.

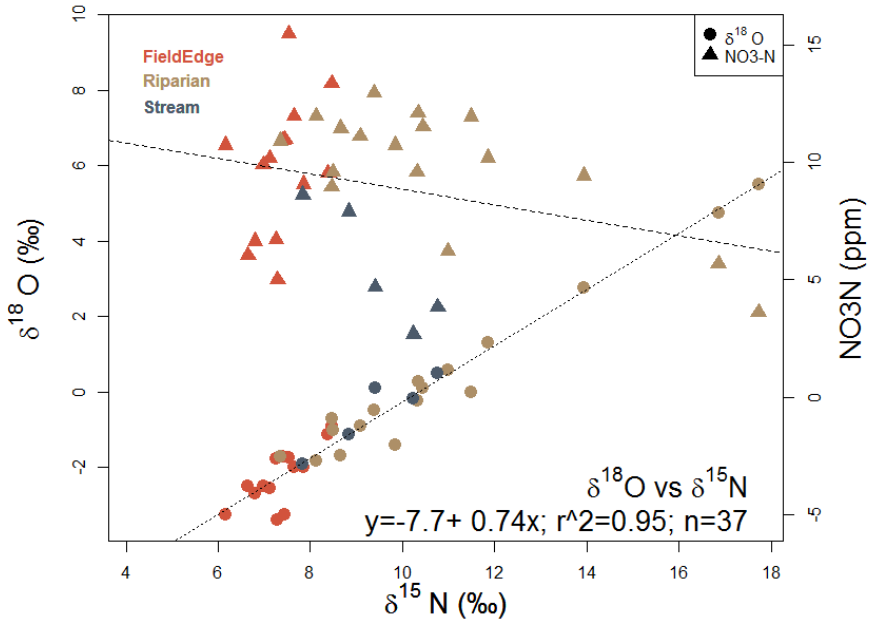

Figure 11 – $\delta^{18}O$ (circles) and NO_3-N (triangles) in the Riparian Area as a function of , $\delta^{15}N$. Red = Field edge, brown = riparian groundwater, blue = stream (Figure 9)

RESULTS AND CONCLUSIONS

The denitrification rates we calculated from the isotopic mass balance are given in Table 7. The observed values range from 33 to 990 kg-N ha^{-1} yr^{-1}. The negative value is physically unrealistic and likely the result of assumptions in the calculations.

Table 7 - Modeled and Observed Areal Denitrification Rates

Date	Observed Values (kg-N ha^{-1} yr^{-1})
6-14-2012	411
7-2-2012	990
8-2-2012	459
8-14-2012	177
8-15-2012	427
9-20-2012	190
10-23-2012	41
10-30-2012	-11
11-06-2012	33

We compared the predicted denitrification rates (using the modeled hydrology) in Riparian Area A (Figure 9) with the calculated values from the isotopic / mass-balance method. The results do

not compare well, with the model consistently under-predicting the observed rates (Figure 12). We attribute this mismatch to three potential causes, each of which needs further study.

First, we suspect that the hydrologic model may underpredict the riparian soil moisture, particularly during the dryer portions of the summer. Exploration of this would involve closer examination of the water table and soil moisture dynamics in this wettest area of the landscape.

Second, our observed estimates of the riparian areas are based on the assumption that the riparian area is at steady state and the conclusion that denitrification is the primary transformative process for NO_3^-. We have assumed that NO_3^- is not adsorbing to the soil in significant quantities. A net adsorption of NO_3^- would decrease the calculated values, bringing them closer to the modeled values. A second process that we've overlooked is dissimilatory nitrate reduction to ammonia (DNRA). Recent studies have indicated that this nitrate reduction process may play a larger role that previously thought, with some evidence of rates comparable to those of denitrification ([45], [46]). We have not seen studies indicating how DNRA would affect the isotopic composition of the remaining nitrate.

Other potential explanations include errors in delineating the riparian area, in classifying the land use or hydrology, in estimating the DOC and NO_3 values in the riparian area, or in measuring the flow through the culvert.

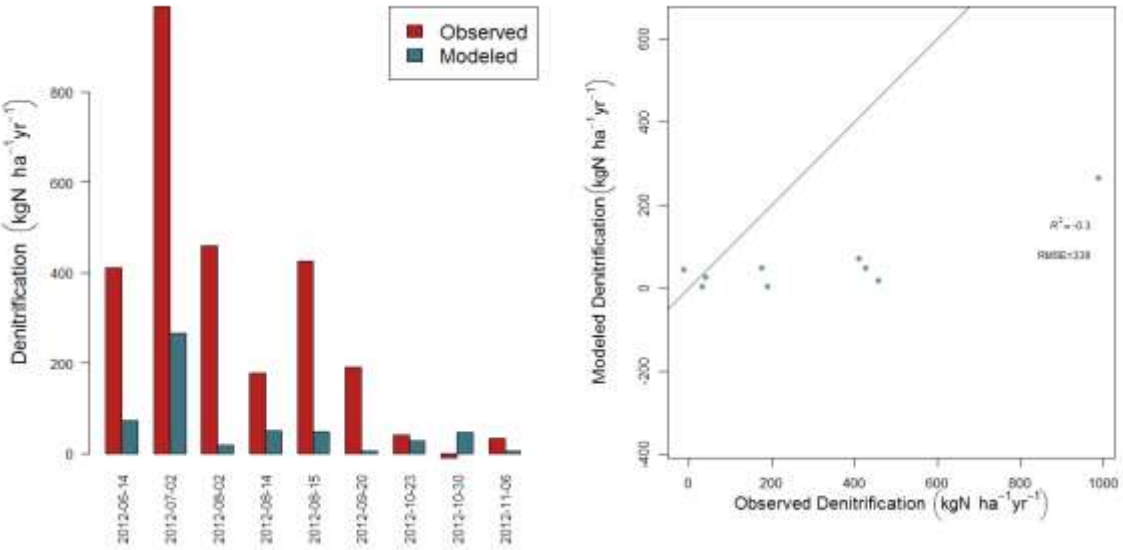

Figure 12 - Isotope Denitrification Results

CHAPTER 3: DENITRIFICATION & CLIMATE CHANGE

INTRODUCTION

Much uncertainty exists in several of the specifics of how global climate is changing, however some census has emerged. For the northeastern USA, it is expected that annual precipitation will increase on the order of 10%, with larger increases in the winter and slight decreases in the summer months [47] by the end of the 21st century. Annual temperatures for the same period are projected to increase approximately 3-5°C, with greater increases in the summer months and lesser increases in the winter months [47]. Although the uncertainty in these estimations is large, the implications of changes of this magnitude are likely significant and it is important that we consider the effects of this scale of change.

The implications of changing climate for denitrification rates are complex due to the complexity of the processes involved. At least two mechanisms of rate changes are possible: changes in residence time and changes in reaction conditions.

Some have suggested that climate change will reduce the residence time of soluble nitrate, thereby reducing the amount that is denitrified and increasing the nitrate load to streams [48], [49]. With this change mechanism, nitrate-rich water flows more quickly through the landscape, reducing the time spent in areas conducive to denitrification and thereby reducing the amount of nitrate that is denitrified. Others have noted the potential complications of disconnecting zones of nitrate loading from zones of denitrification [50]. This change mechanism would decrease the residence time to zero, reducing denitrification rates to near zero.

From the reaction environment side, soil temperature and degree of saturation have been shown to be important controls on denitrification rates ([6] [8]). The increased temperatures of

the climate projections would be expected to have a rate-increasing effect on denitrification. Increased precipitation would be expected to increase the degree of soil saturation, however, increased temperatures might counteract this due to increased evapotranspiration.

The objective of this study is to examine the effects of changing precipitation and temperature on denitrification rates. Specifically, we seek to answer three questions: 1) How might the magnitude and spatial and temporal patterns of denitrification change?, 2) What are the relative strengths of precipitation and temperature as drivers of these changes?, and 3) How might changes in the patterns of precipitation and temperature affect denitrification rates?

METHODS

To address these questions, we used the simple denitrification model coupled with a semi-distributed hydrologic model described in chapter 1.

BASELINE CLIMATE SERIES

Typically, future climate projections are relative to a baseline period of 1961-1990 [47], however the on-site weather station at our study site did not come online until 2004 so we generated our baseline data series using historic weather data from the NOAA National Climate Data Center, Station GHCND: USC00304174 (ITHACA CORNELL UNIVERSITY) [51], which is in Ithaca, NY, 13 miles to the west. A comparison of the concurrent weather data from Ithaca and Harford (2005-2012) indicated that Harford is approximately 0.9 ^{o}C colder than Ithaca, and annually receives 3 cm more rain and has 15 more days of rain (Table 8). Over the eight year comparison period, Harford experienced 3 more rainy days month^{-1} in the wetter months of January – April, and 0.5 more rainy days month^{-1} in the months of May through December (data not shown). We assumed this same relationship held in the baseline period of 1961-1990. To create a historic baseline for Harford, NY (1961-1990) from the historic Ithaca weather, we decreased the daily minimum, maximum, and average temperatures by 0.9 °C, increased the

daily precipitation depth by 5%, and randomly added 0.5 days of rain month^{-1} for May – December and 3 days rain month^{-1} for January – April.

Table 8 - Differences in Annual Climate between Ithaca and Harford

Year	Rainless Days	Precip (cm)	Tmax(C)	Tmin(C)
2005	29	0.87	1.00	1.21
2006	-3	3.35	1.02	1.02
2007	28	-9.3	0.85	0.80
2008	8	-5.39	1.10	1.01
2009	43	-11.75	0.90	0.69
2010	16	5.29	0.87	1.09
2011	3	-3.87	0.63	0.88
2012	18	-2.21	0.92	1.10

FUTURE CLIMATE SERIES GENERATION

We used three future emissions scenarios (B1, A2, and A1F1) developed by the Intergovernmental Panel on Climate Change (IPCC) as the basis for generating our future climate series. Briefly, A1F1 is a scenario of rapid economic growth with an emphasis on fossil fuels, A2 is a scenario of slower, more fragmented economic growth focused at the regional and local scale, and the B1 scenario involves a rapid shift in economic structures such that material resource use decreases and efficiency increases [52].

Table 9 - Temperature and Precipitation Projects for the Northeastern United States for 2070-2099 [47]

Series	Annual Temp (°C)	Summer Temp (°C)	Winter Temp (°C)	Annual Precip (%)	Summer Precip (%)	Winter Precip (%)
Baseline	-	-	-	-	-	-
B1	2.9	2.4	1.7	7	(-1)	12
A2	4.5	4.3	3.7	9	(-2)	14
A1F1	5.3	5.9	5.4	14	0	30
A1F1 – Temp	5.3	5.9	5.4	-	-	-
A1F1 - Precip	-	-	-	14	0	30

Projections for annual, summer and winter shifts to mean temperature and precipitation (Table 9) were taken from Hayhoe et al. [47]. We modified the daily baseline summer and winter temperature and precipitation values by the projected shifts to the summer and winter mean values. Then, we adjusted the spring and fall values until the new annual mean matched the projected annual mean values. This method, known as the "delta method," has the advantage of simplicity and has been shown to be relatively successful at modeling the observed climate. The drawback of the delta method is that it can mis-predict extreme events ([53], [54] [55]).

The "Precipitation Only" and "Temperature Only" series were generated by using the precipitation (or temperature) series from the A1F1 scenario and the temperature (or precipitation) series from the baseline data.

One drawback of the delta method of downscaling is that it assumes the future weather patterns will be the same as the current weather patterns. To explore the influence of changing weather patterns on denitrification, we generated three hypothetical weather series with the same annual and seasonal means as the A1F1 series. In the Random series, precipitation amounts randomly sampled from a distribution of double the A1F1 seasonal values occur on randomly selected days from the season in question. Average daily temperature values for this series were generated randomly using the monthly mean and standard deviation. Daily maximum and minimum temperatures were generated from daily temperature ranges, determined randomly using the monthly mean daily temperature range. In the Mean series, daily precipitation and temperature values were taken from the mean daily values from the A1F1 scenario. In the Cyclic series, temperature and precipitation patterns occur in 5 day cycles. Again, based on the A1F1 series, each month's precipitation is uniformly divided among five consecutive days in the month (all other days have no precipitation) and daily temperatures are selected as in the Random series, except that the daily minimum, maximum, and average temperatures remain constant for five days before changing.

RESULTS AND DISCUSSION

We compared the annual and seasonal precipitation and soil temperature (Figure 13) to verify the weather series generation process. Both the annual and seasonal temperature changes matched the expectations. The number of low flow days increased and the stream discharge decreased, especially in the A2 scenario (Figure 14B). The summer decrease in soil moisture was came earlier and was larger (Figure 15).

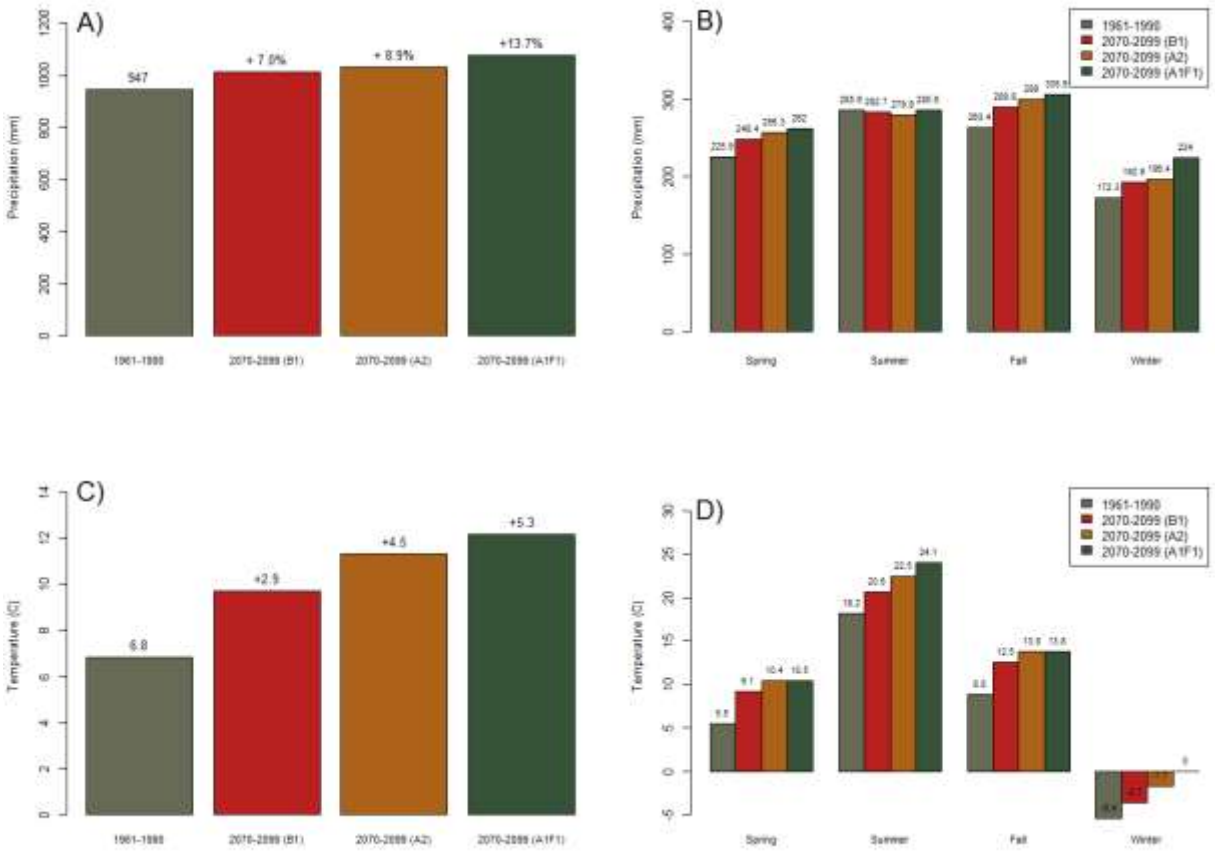

Figure 13 - Annual (A) and Seasonal (B) Precipitation and Annual (C) and Seasonal (D) Soil Temperature with the four climate scenarios. This confirms that our weather series generation process duplicated the projected changes.

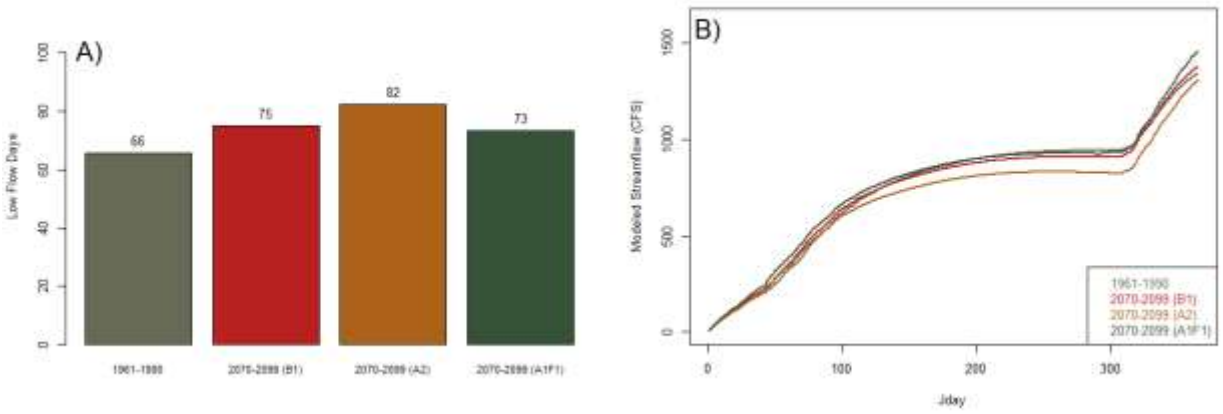

Figure 14 – A) All three future climate scenarios resulted in more low flow days annually (days in which the modeled discharge was below the 18% threshold in the baseline scenario). B) Mean cumulative stream discharge in the four scenarios. Scenario A2 resulted in a decreased modeled stream discharge beginning in the spring season.

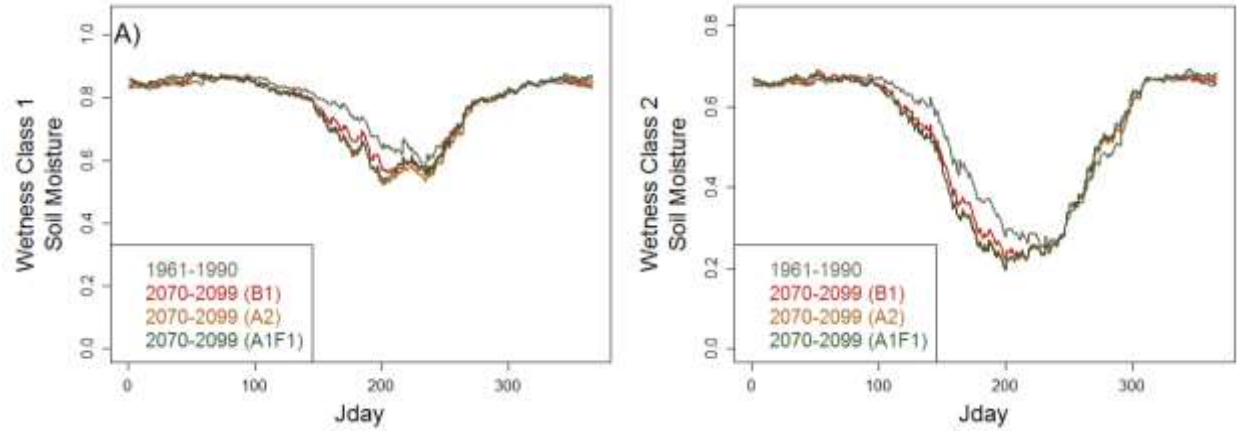

Figure 15 – Soil Moisture in Wetness Classes 1 & 2: As expected, all three future climate scenarios result in an earlier and larger drop in Soil Moisture, both in Wetness Class 1, where the soil is recharged by the groundwater(A), and in Wetness Class 2 where the model does not include recharge (B).

COMPARISON OF BASELINE CLIMATE AND B1, A2, & A1F1 SCENARIOS

With all future scenarios, our model predicts an increase in denitrification rates relative to the baseline weather. The greatest increase is with scenario A1F1 (6.7 kg-N ha^{-1} yr^{-1}, 81% increase) and the smallest increase is with scenario B1 (3 kg-N ha^{-1} yr^{-1}, 35% increase) (Figure 16). In all four weather scenarios, the highest watershed-wide denitrification rates occur during the spring season. As with the annual rates, our model predicts increased seasonal denitrification rates for all three scenarios, with the greatest increases in scenario A1F1 (Figure

17). There is a slight shift in the seasonal pattern of denitrification. All three scenarios show a decrease in the summer fraction of annual denitrification. In scenarios B1 and A2, the spring fraction increases relative to the baseline conditions, whereas in scenarios A1F1 the increase is primarily in the winter season (Figure 17).

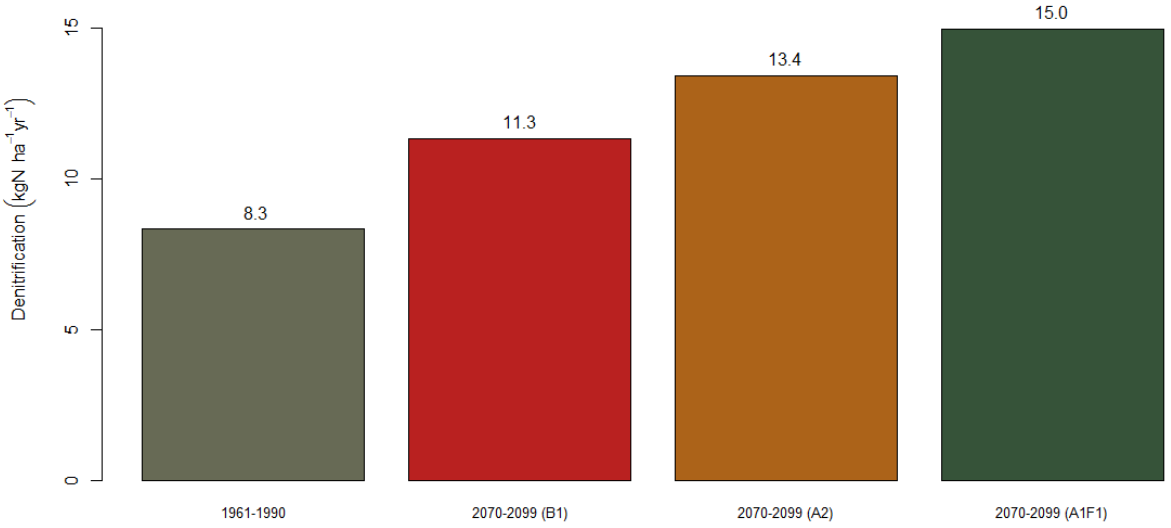

Figure 16 - Annual Modeled Denitrification Rates

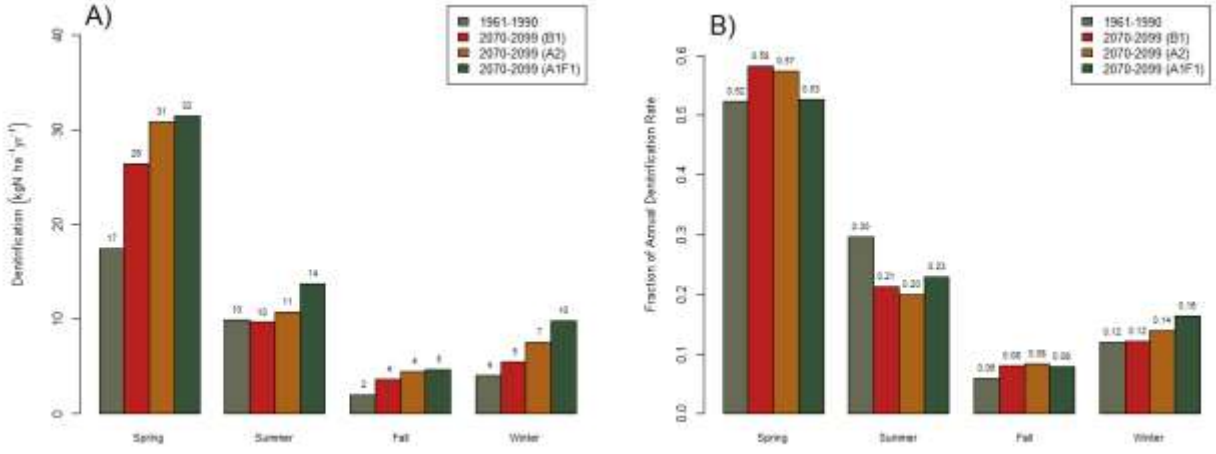

Figure 17 - Seasonal Rates and Seasonal Fraction of Annual Rates – Seasonally, the greatest increases in denitrification rates are during the spring (A), and there is a slight increase in the spring fraction of annual denitrification in the B1 and A2 scenarios (B).

WETNESS CLASS 1 DENITRIFICATION RATES

In contrast to the watershed-wide rates, the denitrification rates in the wettest areas are high in the summer season, as well as during the spring. During the summer, this wettest class remains sufficiently wet to maintain anaerobic conditions, while the rest of the watershed dries substantially (Figure 18A). The locations where wetness class 1 overlaps with wetland vegetation and soils create unique and important biogeochemical hotspots. In the baseline scenario, 45% of the annual denitrification from wetness class 1 occurs during the summer, with an additional 38% occurring during the spring. With all three future scenarios, the summer fraction decreases and the spring fraction increases, though the changes with the A1F1 scenario are much less than with the A2 & B1 (Figure 18B). During the spring, when much of the watershed is wet enough to create anaerobic conditions, wetness class 1 contributes 25-31% of the denitrification from the watershed, with a lower fraction in the baseline weather conditions and the highest fraction associated with the highest emissions, i.e., the A1F1 scenario. As the rest of the watershed dries in the summer season, the wetness class 1 contribution increases to 52-68%, with the higher class 1 fractions from the future climate scenarios (Figure 18C). Annually, the wettest class contributes 34-40% of the annual denitrification, with high percentages in the higher emissions scenarios (Figure 18D).

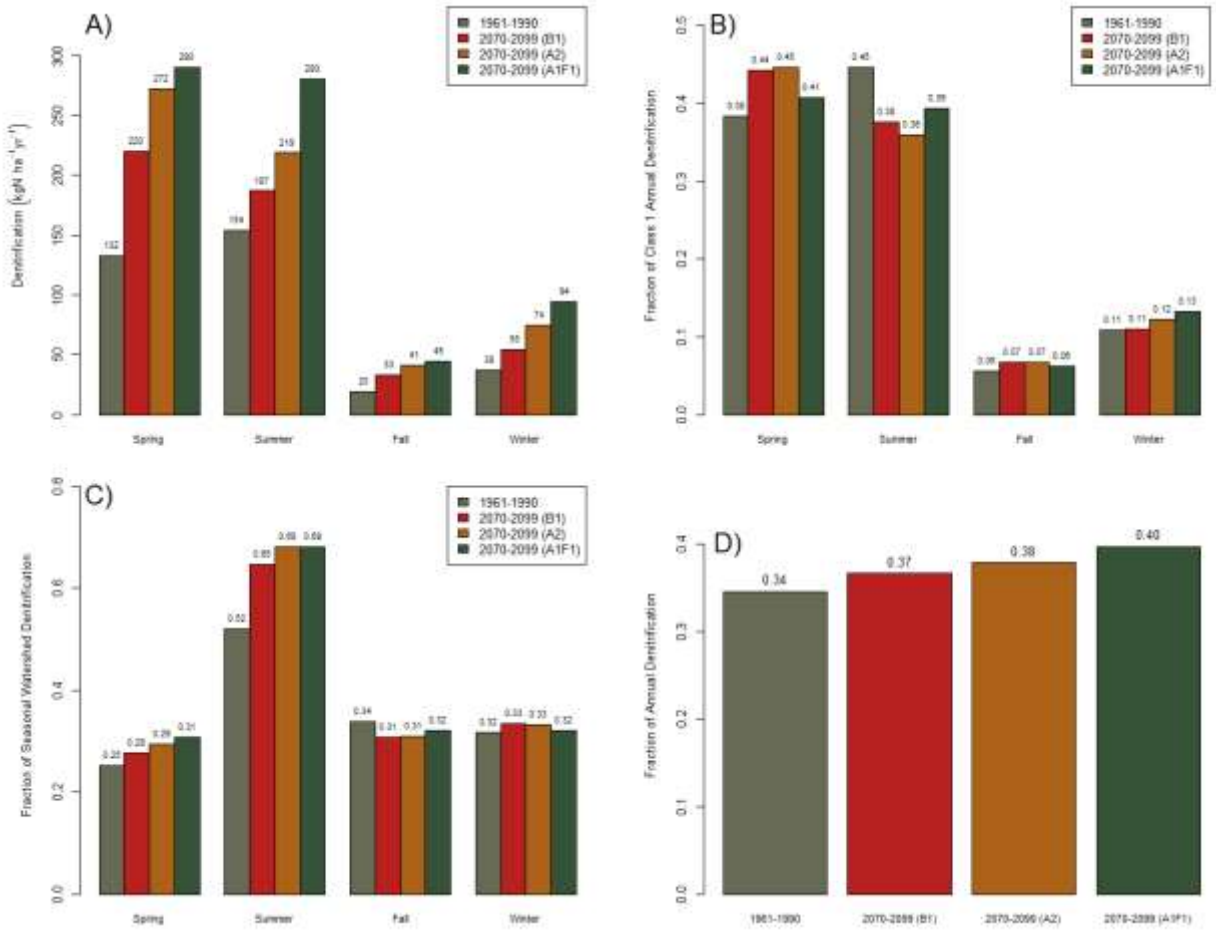

Figure 18 – Denitrification in Wetness Class 1 (A – TOP LEFT: Seasonal Denitrification Rates, B – TOP RIGHT: Seasonal Fraction of Annual Class 1 Denitrification, C – BOTTOM LEFT: Class 1 Fraction of Watershed-wide Seasonal Rate, D – BOTTOM RIGHT: Class 1 Fraction of Annual Watershed-wide Rate)

PATTERNS OF CHANGES

The spatial pattern of changes in annual denitrification rates follows the same pattern as the baseline denitrification rates (Figure 19); specifically, areas with lower baseline rates have small increases and areas with higher baseline denitrification rates have larger increases. These changes range from 1-3 kg-N ha^{-1} yr^{-1} in much of the watershed, to nearly 300 kg-N ha^{-1} yr^{-1} in the riparian wetlands, i.e., the areas that are wetlands and the wettest wetness class.

Temporally, the watershed-wide rates of denitrification follow the same basic pattern with all climate scenarios, though the future scenarios have higher rates, especially during the spring

season (Figure 20). Our model suggests that most denitrification rates will scale upwards due to increased temperature, but that some will decrease due to decreased soil moisture.

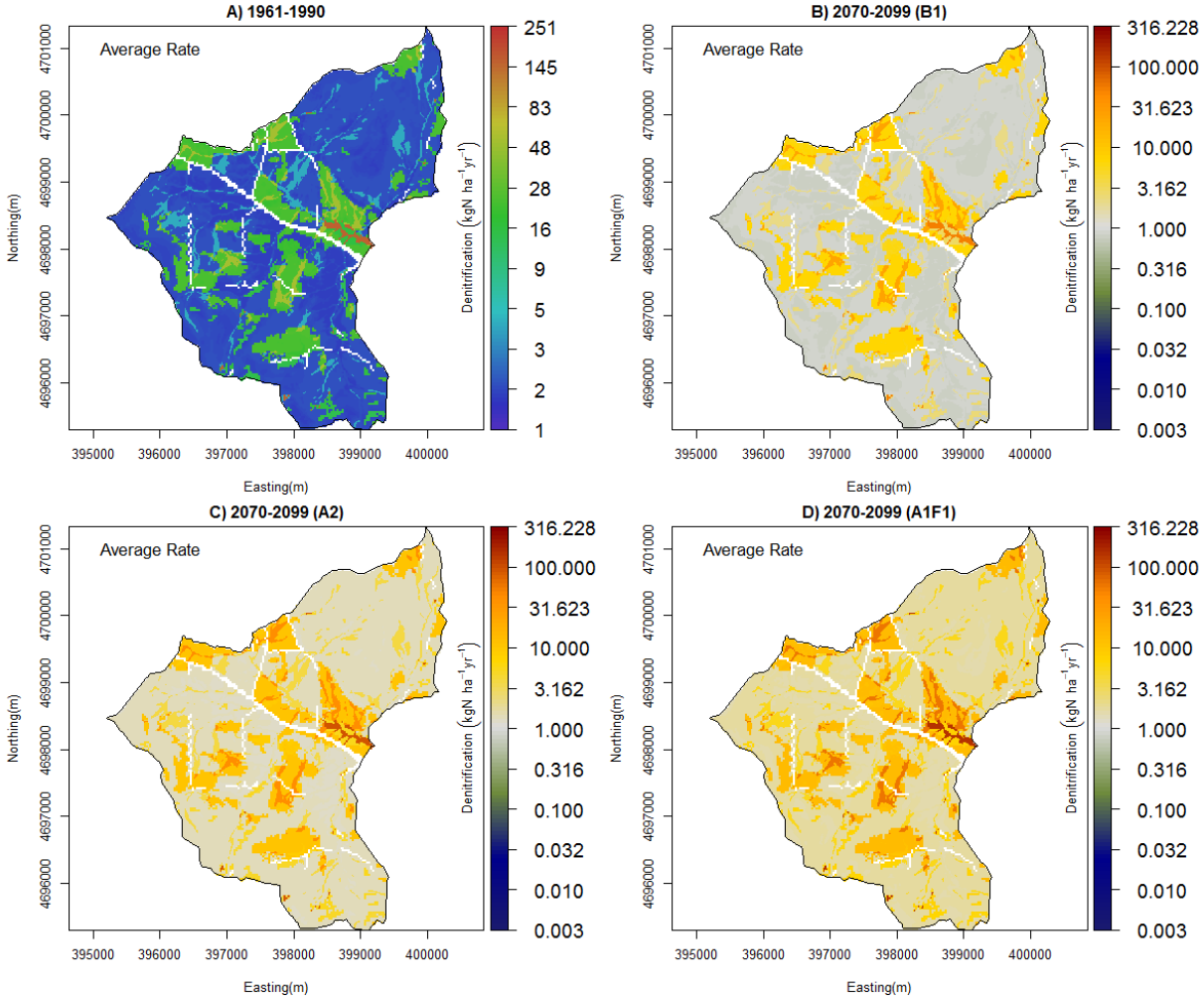

Figure 19 - Spatial Patterns of Denitrification Rates and Changes- A) Average Annual Modeled Denitrification Rates across the Watershed in the Baseline Series, B-D) Changes in the Average Annual Denitrification Rates in the Three Climate Scenarios

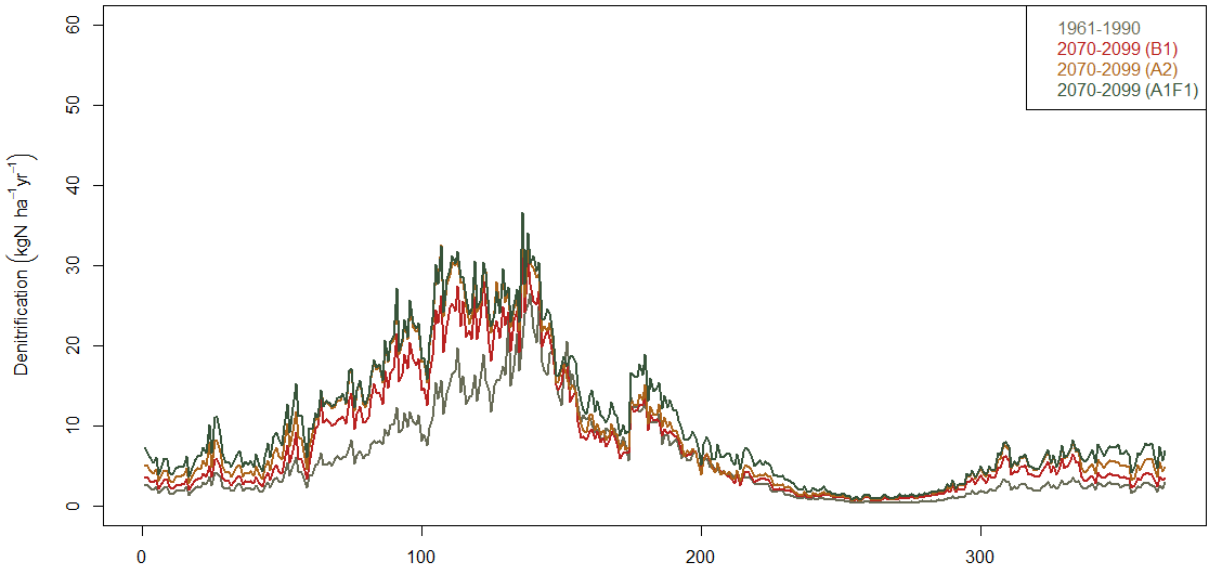

Figure 20 – Average Watershed-wide Denitrification Averaged by *JDay*

SLIGHT INCREASE IN DAYS WITHOUT DENITRIFICATION

In all but the wettest areas of the watershed, we project an increase in the number of days annually on which no denitrification occurs (Figure 21). With the baseline weather, most of the watershed contributes no denitrification on 89 – 92 days year^{-1}. This increases to 102-110 days year^{-1} in the future scenarios, with slightly greater increases in the A2 scenario. The wettest areas underwent much smaller absolute changes, from a baseline rate of 5 days annually, to 14 days in A2 and 12 days in B1 and A1F1. This increase is due to a decrease in anaerobic conditions resulting from drier soils.

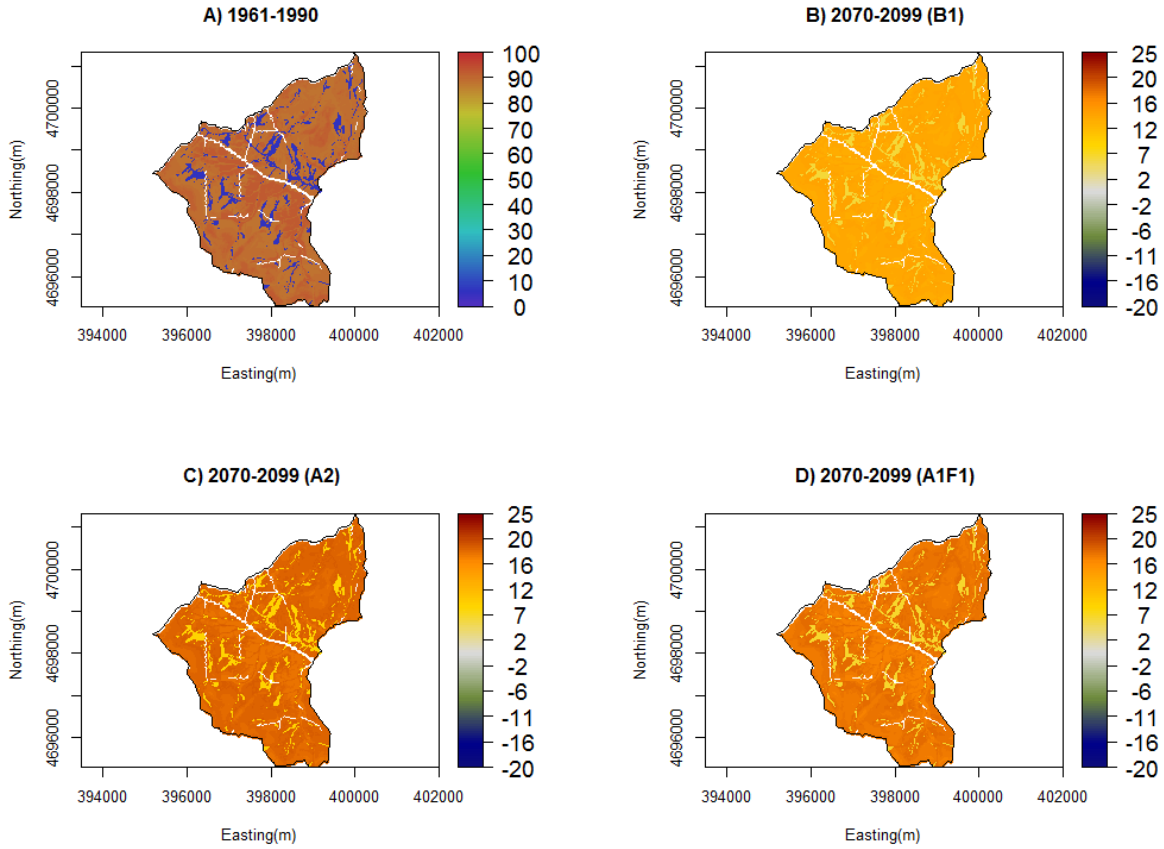

Figure 21 - Annual Days with No Denitrification - A) Baseline Series, B-D) Change from the Baseline Scenario

Relative Influence of Changes in Precipitation and Temperature

To examine the relative influence of changes in precipitation and temperature, we created a future weather series that combined the precipitation from the A1F1 scenario with the temperature from the baseline series, and another that combined the temperature from the A1F1 scenario with the precipitation from the baseline series. The annual denitrification rate increased with both new scenarios, but the increase is much greater with the temperature series. The increase from the baseline scenario to the A1F1 scenario is greater than the combination of the increases in the separate temperature and precipitation scenarios (Figure 22).

Spatially, both the temperature and precipitation scenarios mirror the pattern of changes in the A1F1 scenario, but the magnitude is very different (Figure 23). The A1F1 scenario exhibits changes of 2-13 kg-N ha^{-1} yr^{-1} in most of the watershed, and increases of 150 kg-N ha^{-1} yr^{-1} in the riparian wetlands. In the temperature scenario, these changes are slightly more modest, 1 – 9 and 80 kg-N ha^{-1} yr^{-1} respectively, however the precipitation scenario values are much closer to the baseline, with increases of 0 – 1 kg-N ha^{-1} yr^{-1} in most areas and 23 kg-N ha^{-1} yr^{-1} in the riparian wetlands.

Increases in denitrification rates with the A1F1 scenario are greater than the combined increases from the temperature- and precipitation-alone scenarios. In part, this is due to the multiplicative form of the denitrification model, but is it also due to a counteracting effect the respective changes have on the watershed hydrology. Temperature increases decrease the soil moisture, both watershed-wide and in the wettest areas, whereas precipitation increases increase the soil moisture, such that the combined effects are moderated (Figure 24). Similarly increased temperatures result in decreased cumulative stream discharge (Figure 25).

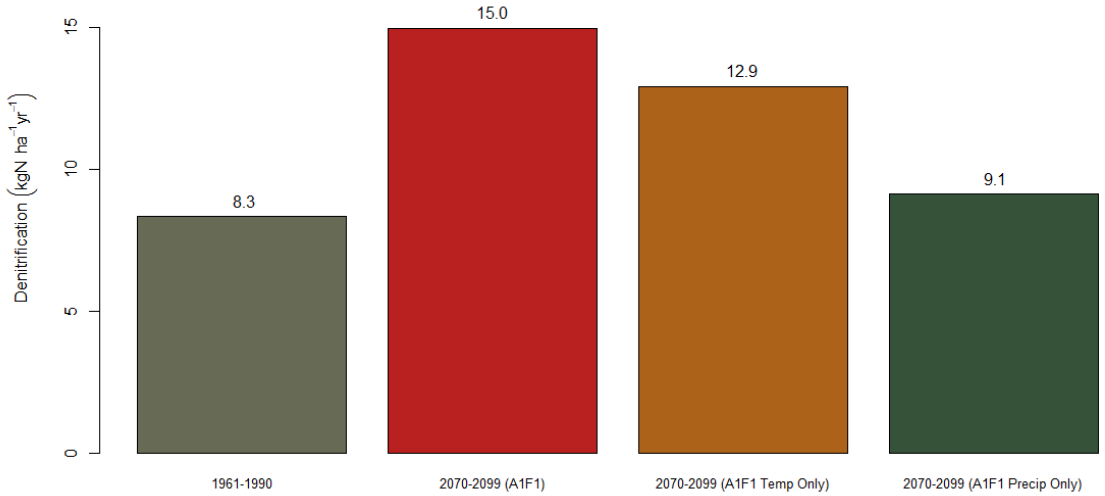

Figure 22 - Relative Effects of Temperature and Precipitation Changes on Annual Denitrification Rates – Projected Temperature changes account for the majority of the change between the Baseline scenario and the A1F1 scenario, with much smaller changes between the Baseline scenario and the A1F1 Precip Only scenario.

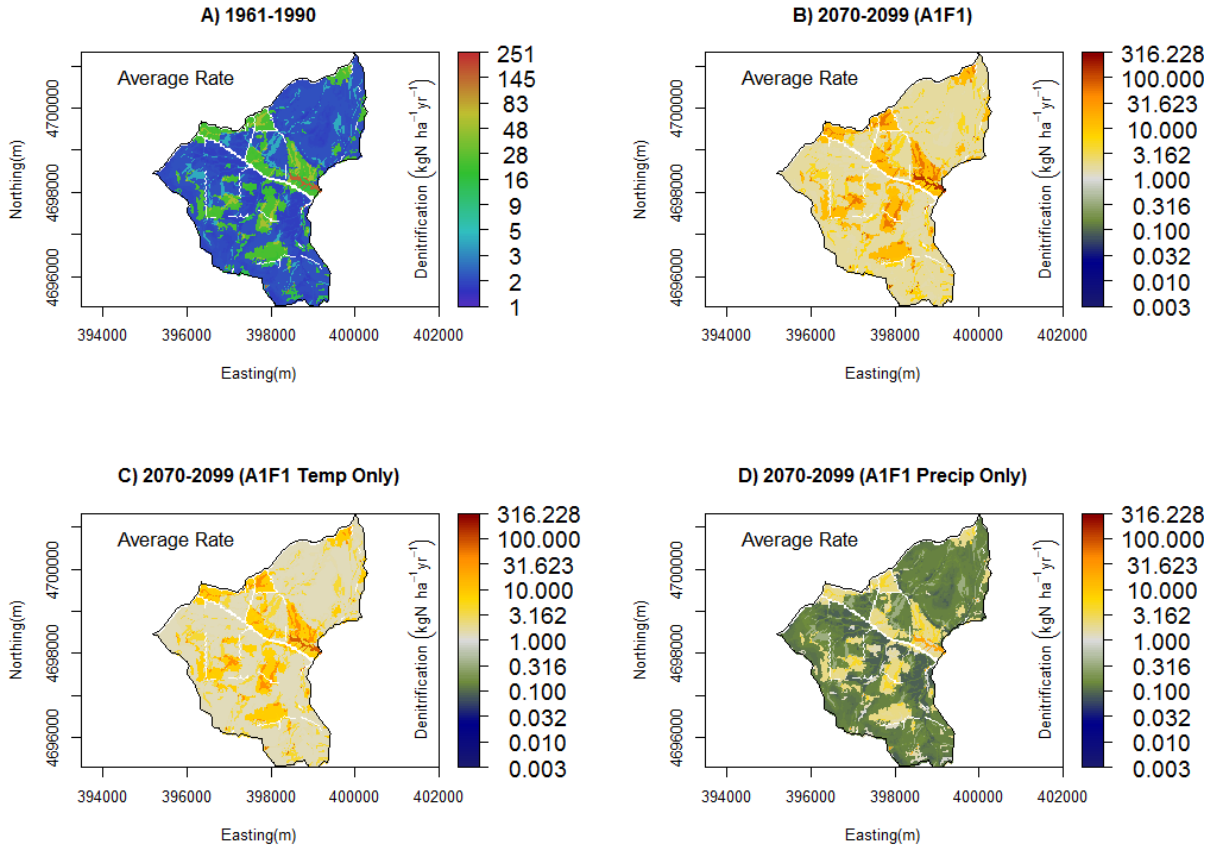

Figure 23 - Spatial Patterns of Precipitation and Temperature Influence - A) Average Annual Modeled Denitrification Rates across the Watershed in the Baseline Series, B-D) Changes in the Average Annual Denitrification Rates in the A1F1, A1F1 Temperature, and A1F1 Precipitation Scenarios

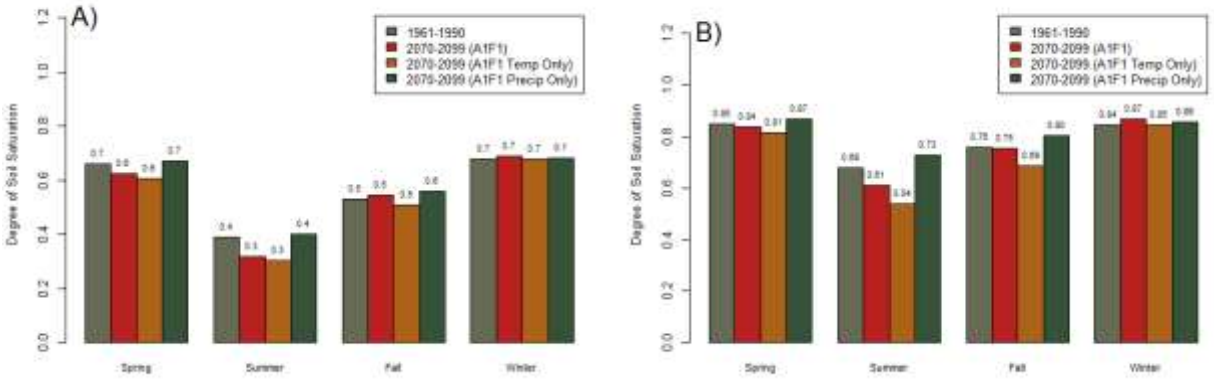

Figure 24 – Influence of Temperature and Precipitation on Seasonal Soil Moisture Watershed-wide (left) and in Wetness Class 1 (right)

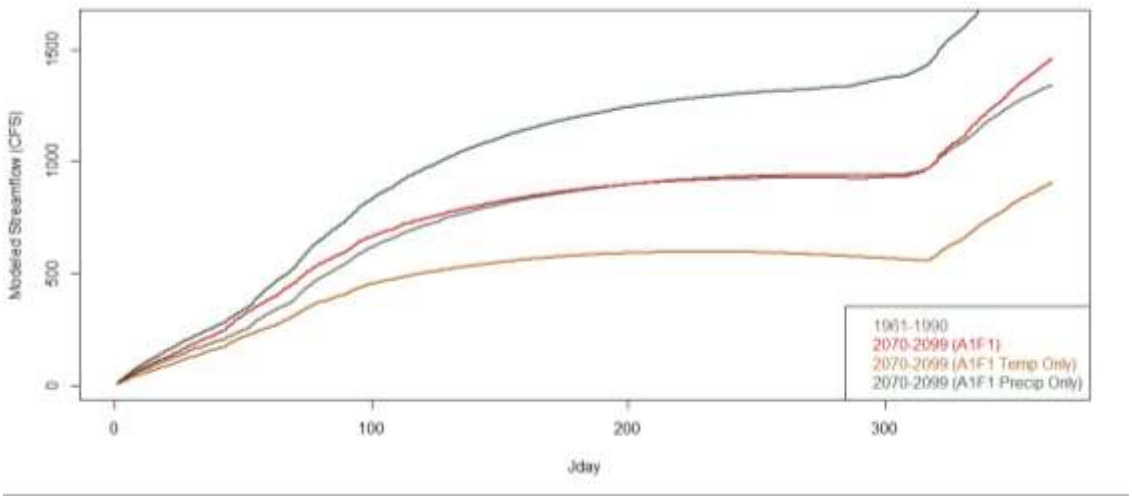

Figure 25 – Influence of Temperature and Precipitation Changes on Cumulative Stream Discharge

EFFECTS OF WEATHER PATTERNS

Our final analysis sought to address the effects of temperature and precipitation patterns on denitrification rates. We generated three more weather series, each with the same seasonal mean temperature and precipitation as the A1F1 scenario, but with different daily patterns. We recognize that actual weather patterns are more complex and interrelated than in these series, however these hypothetical patterns allow us to answer some questions about changing weather patterns.

The spatial and temporal patterns of denitrification rates did not vary much among the A1F1, Random, and Cyclic scenarios. The Annual Denitrification Rate and Seasonal Fractions were similar (Figure 26), as were the spatial patterns of annual rates (Figure 27), and the number of days on which no denitrification was projected (Figure 28). The denitrification rates from the Mean scenario were a bit different. The annual rate was lower (Figure 26), the seasonal rate was higher in the spring and lower in the summer and fall (Figure 26),the spatial pattern exhibits decreases in the wet areas where the other scenarios show increases (Figure 27), and there are more than forty more days annually without denitrification in most of the watershed (Figure 28).

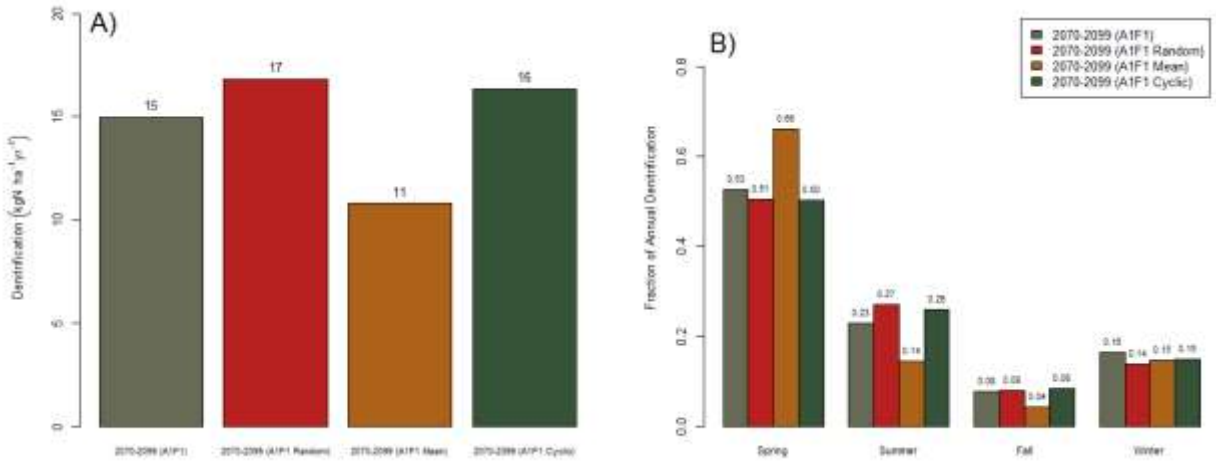

Figure 26 - Annual Denitrification Rate (A) and Seasonal Fraction (B) with Four Weather Patterns

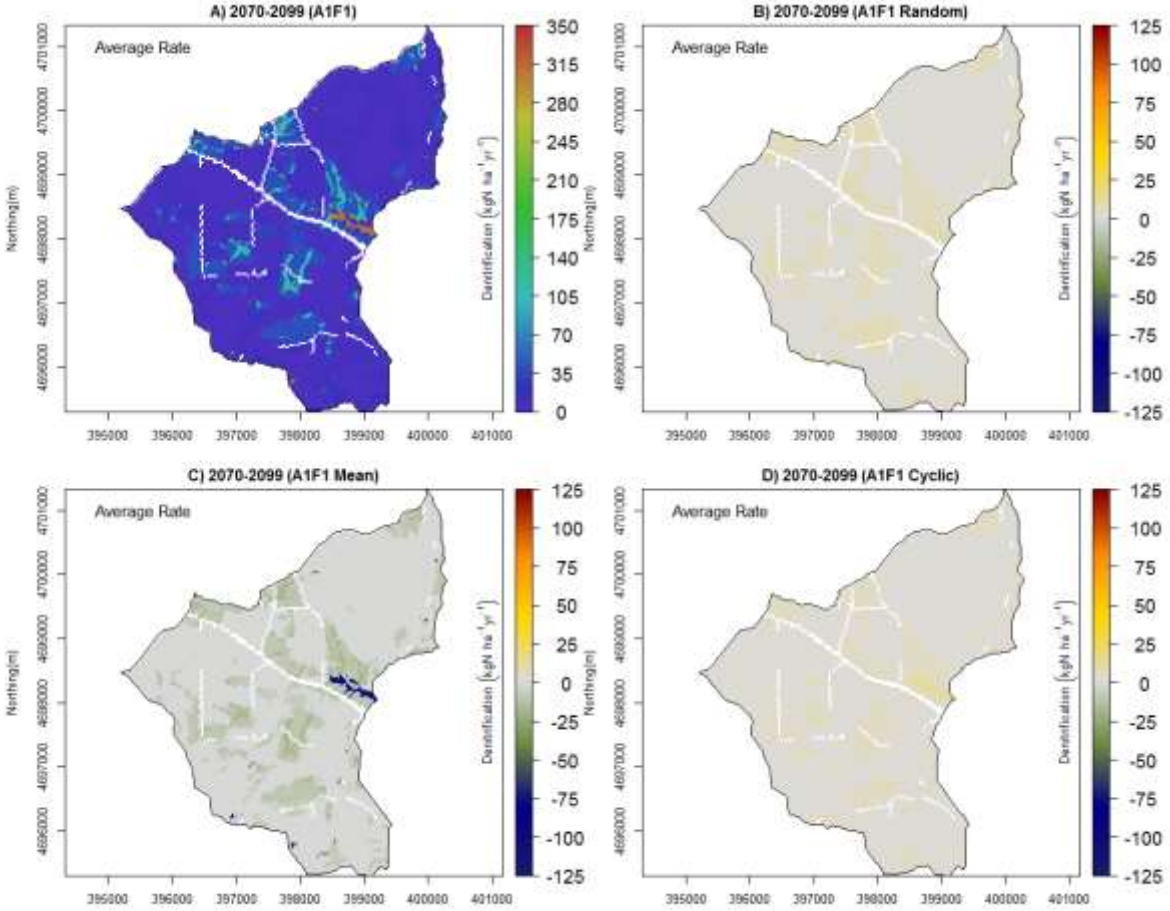

Figure 27 - Spatial Pattern of Denitrification Rates and Changes in the Rates - A) Average Annual Modeled Denitrification Rates across the Watershed in the A1F1 Scenario, B-D) Changes in the Average Annual Denitrification Rates in the Random, Mean, and Cyclic variations of the A1F1 Scenario

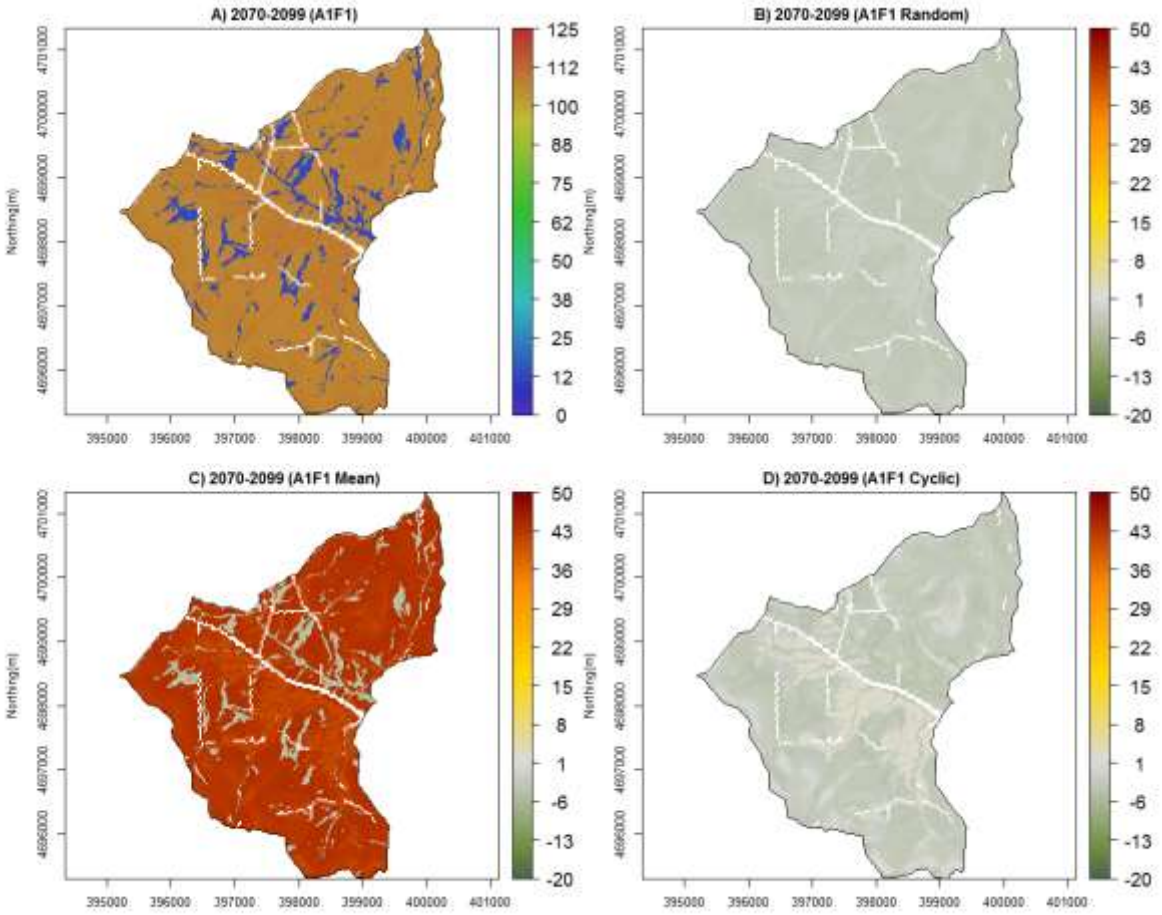

Figure 28 - Annual Days on which No Denitrification is Projected - A) Average Days Annually without Denitrification across the Watershed in the A1F1 Scenario, B-D) Changes in the Number of Denitrification-less Days in the Random, Mean, and Cyclic variations of the A1F1 Scenario

CONCLUSION

In conclusion, we project that climate change will increase annual rates of denitrification in this watershed. The greatest projected increases are in the areas and seasons with the highest baseline rates, with smaller increases in those with lower baseline rates. We saw no notable changes in the spatial patterns of denitrification. We found that changing temperature is be a much stronger driver of change to denitrification rates than changing precipitation, and that these changes are only moderately influence by the daily weather patterns we examined.

APPENDICES

APPENDIX 1: GROUNDWATER FLOW CALCULATIONS

We calculated the volume of water leaving the catchment via groundwater flow as a function of the angle of the hydraulic gradient. We based this calculation on observations from the northeast corner of the catchment and assumed the catchment is symmetrical in this regard.

HYDRAULIC HEAD CALCULATIONS

We measured the depth to the water table at 3 wells (Figure 29) at the field edge of the Riparian Area on 5 occasions between July and September 2012, and added this to records for these wells from Geohring [21]. The angle of the groundwater gradient was calculated:

$$\phi = A + B \quad [a]$$

$$A = \tan^{-1}\left(\frac{{}^{h_2-h_1}/_{l_{1,2}}}{{}^{h_3-h_1}/_{l_{1,3}}}\right) \quad [b]$$

$$B = \tan^{-1}\left(\frac{\Delta y_{1,3}}{\Delta x_{1,3}}\right) \quad [c]$$

Where *A* is the angle gradient and the line connecting wells 1 & 3; *B* is the angle between that line due East; h_1, h_2 & h_2 are the hydraulic head (m) at wells 1,2 & 3; $l_{1,2}$ & $l_{1,3}$ are the distances (m) between wells 1 & 2 and 1&3; $\Delta x_{1,3}$ & $\Delta y_{1,3}$ are the changes in Easting (m) and Northing (m) between wells 1 & 3. From the observed data, we calculated a relationship between Φ and the degree of saturation in wetness class 2 (Figure 30A): as the soil dries, Φ increases, directing more of the flow parallel to the stream rather than towards the stream. We then calculated the relationship between Φ and the stream discharge residuals when groundwater flow was left out of the model (Figure 30B) and assumed this volume of water left the catchment via groundwater flow.

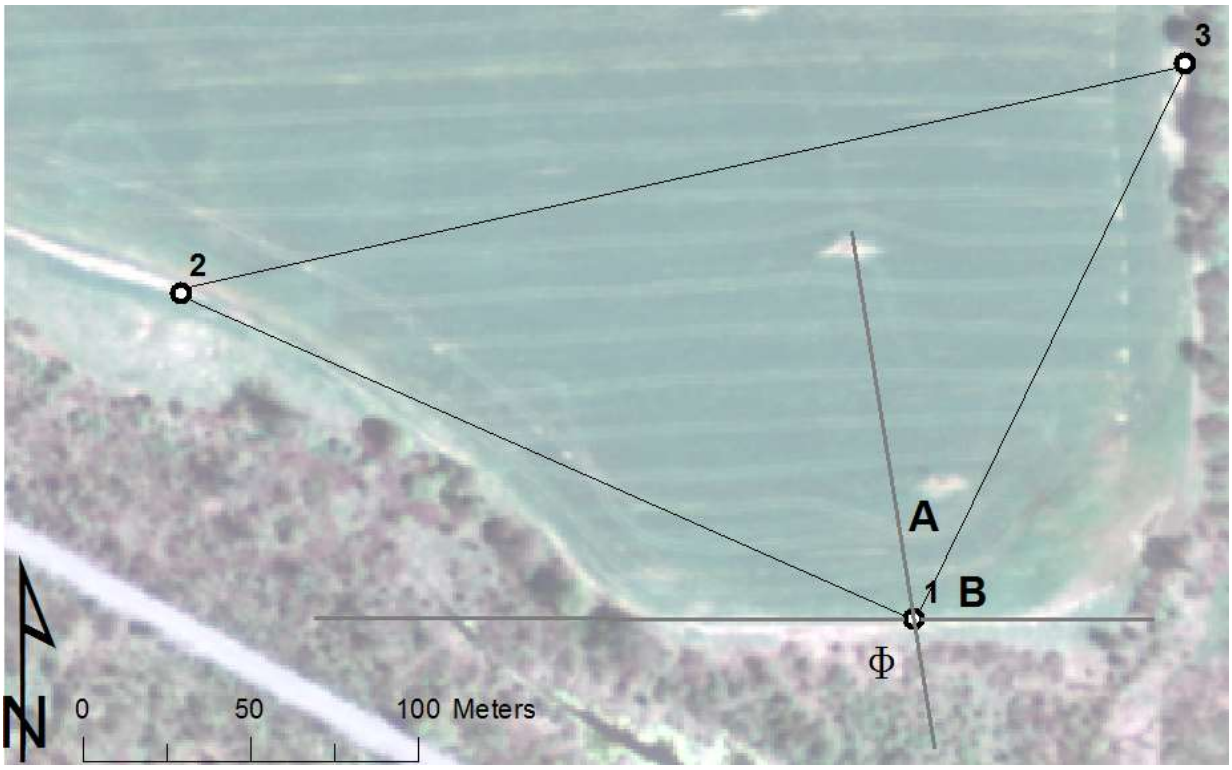

Figure 29 - Location of Groundwater Sampling Wells

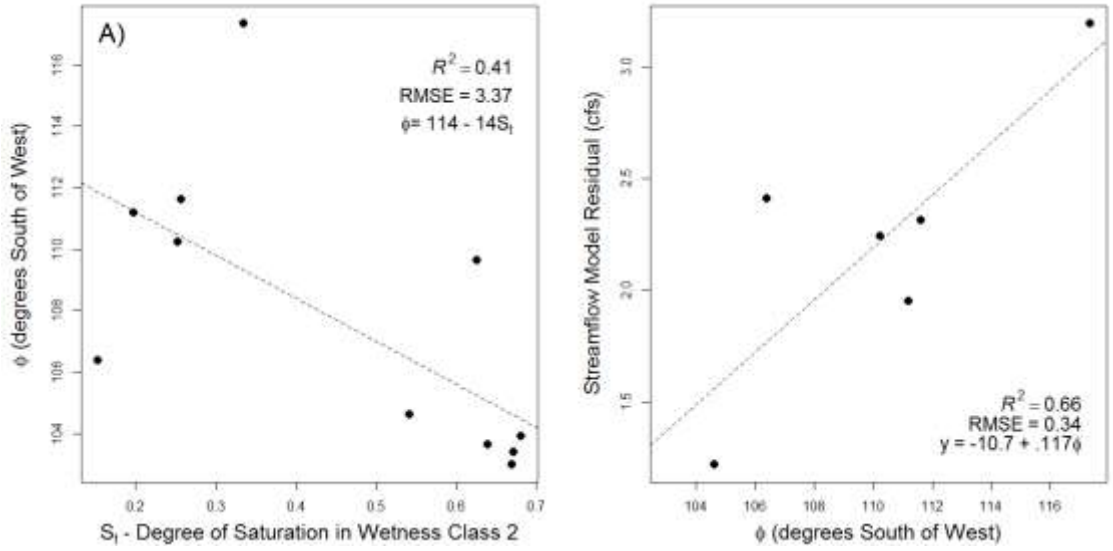

Figure 30 - A) Relationship between Φ (groundwater flow angle) and the Soil Saturation in Wetness Class 2; B) Relationship between Φ and the Streamflow Residual

REFERENCES

[1] EPA, "Effects of Nitrogen and Phosphorus Pollution," 29 9 2011. [Online]. Available: http://water.epa.gov/scitech/swguidance/standards/criteria/nutrients/effects.cfm. [Accessed 7 11 2011].

[2] N. Van Breeman, E. W. Boyer, C. L. Goodale, N. A. Jaworski, K. Paustian, S. P. Seitzinger, K. Laitha, B. Maer, D. Van Dam, R. W. Howarth, K. J. Nadelhoffer, M. Eve and G. Billen, "Where did all the nitrogen go? Fater of nitrogen inputs to large watershed in the northeastern USA," *Biogeochemistry,* pp. 267-293, 2002.

[3] EPA, "Basic Information about Nitrate in Drinking Water," United States Environmental Protection Agency, 21 5 2012. [Online]. Available: http://water.epa.gov/drink/contaminants/basicinformation/nitrate.cfm. [Accessed 29 5 2013].

[4] P. M. Groffman, M. A. Altabet, J. Bohlke, K. Butterbach-Bahl, M. B. David, M. K. Firestone, A. E. Giblin, T. M. Kana, L. P. Nielsen and M. A. Voytek, "Methods for Measuring Denitrification: Diverse Approaches to a Difficult Problem," *Ecological Applications,* pp. 2091-2122, 2006.

[5] E. W. Boyer, R. B. Alexander, W. J. Parton, C. Li, K. Butterbach-Bahl, S. D. Donner, R. W. Skaggs and S. J. Del Grosso, "Modeling Denitrification in Terrestrial and Aquatic Exosystems at Regional Scales," *Ecological Applications,* pp. 2123-2142, 2006.

[6] M. Heinen, "Simplified denitrification models: Overview and properties," *Geoderma,* pp. 44-463, 2006.

[7] T. Steenhuis, J. -Y. Parlange, W. E. Sanford, A. Heileg, F. Stagnitti and M. F. Walter, "Can we distinguish Richards' and Boussinesq's equations for hillslopes?: The Coweeta experiment revisited," *Water Resources Research,* vol. 35, no. 2, pp. 589-593, 1999.

[8] C. Henault and J. C. Germon, "NEMIS, a predictive model of denitrification on the field scale," *European Journal of Soil Science,* vol. 51, pp. 257-270, 2000.

[9] M. J. Whelan and C. Gandolfi, "Modelling of spatial controls on denitrification at the landscape scale," *Hydrological Processes,* vol. 16, pp. 1437-1450, 2002.

[10] C. Tague, "Modeling hydrologic controls on denitrification: sensitivity to parameter uncertainty and landscape representation," *Biogeochemistry,* vol. 93, pp. 79-90, 2009.

[11] F. Oehler, P. Durand, P. Bordenave, Z. Saadi and J. Salmon-Monviola, "Modelling denitrification at the catchment scale," *Science of the Total Environment,* pp. 1726-1737, 2009.

[12] NOAA National Climate Data Center, "NY Ithaca 13 E Station Information," [Online]. Available: http://www.ncdc.noaa.gov/crn/report.

[13] K. Addy, D. Kellogg, A. J. Gold, P. M. Groffman, G. Ferendo and C. Sawyer, "In Situ Push-Pull Method to Determine Ground Water Denitrification in Riparian Zones," *Journal of Environmental Quality,* pp. 1017-1024, 2002.

[14] J. Istok, M. D. Humphrey, M. H. Schroth, M. R. Hyman and K. T. O'Reilly, "Single-Well, "Push-Pull" Test for In Situ Determination of Micronial Activities," *Ground Water,* vol. 35, pp. 619-631, 1997.

[15] C. Thornthwaite and J. R. Mather, "The Water Balance," *Publications in Climatology,* pp. 1-104, 1955.

[16] S. W. Lyon, M. T. Water, P. Gerard-Marchant and T. S. Steenhuis, "Using a topographic index to distribute variable source area runoff predicted with the SCS curve-number equation," *Hydrological Processes,* vol. 18, pp. 2757-2771, 2004.

[17] N. Brady and R. R. Weil, The Nature and Properties of Soil: Thirteenth Edition, Upper Saddle River: Prentice Hall, 2002.

[18] C. Priestly and R. Taylor, "On the Assessment of Surface Heat Flux and Evaporation Using Large-Scale Parameters," *Monthly Weather Review,* vol. 100, pp. 81-92, 1972.

[19] M. T. Walter, E. S. Brooks, D. K. McCool, L. G. King, M. Molnau and J. Boll, "Process-based snowmelt modeling: Does it require more input data than temperature-index modeling?," *Journal of Hydrology,* vol. 300, pp. 65-75, 2005.

[20] FAO, "Crop Evapotranspiration - Guidelines for computing crop water requirements," 1998. [Online]. Available: http://www.fao.org/docrep/X0490E/X0490E00.htm. [Accessed March 2012].

[21] L. Geohring, Interviewee, *Personal Communication.* [Interview]. 20 May 2013.

[22] V. Beujouan, P. Durand, L. Ruiz, P. Aurousseau and G. Cotteret, "A hydrological model dedicated to topography=based simulation of nitrogen transfer and transformation: rationale and application to teh geomorphology-denitrification relationship.," *Hydrologic Processes,* vol. 16, no. 2, pp. 493-507, 2002.

[23] N. Brisson, B. Mary, D. Ripoche, M. H. Jeuggroy, F. Ruget, B. Nicoullaud and R. Delecolle, "STICS: a generic model for the simulation of crops and their water and nitrogen balances. I. Theory and parameteriztion applied to wehat and corn.," *Agronomie,* vol. 18, no. 5-6, pp. 311-346, 1998.

[24] USDA NRCS, "Web Soils Survey," [Online]. Available: http://websoilsurvey.nrcs.usda.gov/app/WebSoilSurvey.aspx.

[25] D. Bouldin, *Water quality data for well, stream, and seep samples from the Harford Teaching and Research Farm (Cortland County, NY): 1974-1994.*

[26] H. Dahlke, Interviewee, *Personal Communication.* [Interview]. 2 February 2013.

[27] J. Nash and J. V. Sutcliffe, "River flow forecasting through conceptual models part I - A Discussion of principles," *Journal of Hydrology,* pp. 282-290, 1970.

[28] D. Ardia, K. M. Mullen, B. G. Peterson and J. Ulrish, *'DEoptim': Differential Evolution in 'R'. version 2.2-1,* 2012.

[29] S. Rantz, "Measurement and Computation of Streamflow: Volumes I and II," in *USGS Water Supply Paper 2175*, p. 631.

[30] T. R. Anderson, "Denitrification in riparian zones and other saturated soils of a northeastern agricultural landscape.," *(Doctoral Dissertation),* 2013.

[31] W. E. Dean, "The carbon cycle and biogeochemical dynamics in lake sediments," *Journal of Paleolimnology,* vol. 21, pp. 375-393, 1999.

[32] K. Chan, S. Tarantola, A. Saltelli and I. M. Sobol, "Variance-Based Methods," in *Sensitivity Analysis*, West Sussex, England, John Wiley & Sons, 2000, pp. 167-197.

[33] P. Gilles, B. Iooss and A. Janon, "sensitivity: Sensitivity Analysis," R package version 1.6-1, 2012. [Online]. Available: http://CRAN.R-project.org/package=sensitivity.

[34] D. Moriasi, J. G. Arnold, M. W. Van Liew, R. L. Bingner, R. D. Harmel and T. L. Veith, "Model Evaluation Guidelines for systematic Quantification of Accuracy in Watershed Simulations," *Transactions of the ASABE,* vol. 50, pp. 885-900, 2007.

[35] M. Heinen, "Application of a widely used denitrification model to Dutch data sets," *Geoderm,* vol. 133, pp. 464-473, 2006.

[36] P. M. Groffman, K. Butterbach-Bahl, R. W. Fulweiler, A. J. Gold, J. L. Morse, E. K. Stander, C. Tague, C. Tonitto and P. Vidon, "Challenges to incorporating spatially and temporally explicit phenomena (hotspots and hot moments) in denitrificaiton models,"

Biogeochemistry, vol. 93, pp. 49-77, 2009.

[37] P. M. Groffman, E. A. Cavidson and S. Seitzinger, "New approaches to modeling denitrification," *Biogeochemistry,* vol. 93, pp. 1-5, 2009.

[38] S. Ferrant, F. Oehler, P. Durand, L. Ruiz, J. Salmon-Monviola, E. Justes, P. Dugast, A. Probst and J. Sanchez-Perez, "Understanding nitrogen transfer dynamics in a small agricultural catchment: Comparison of a distributed (TNT2) and a semi-distributed (SWAT) modeling approaches," *Journal of Hydrology,* vol. 406, pp. 1-15, 2011.

[39] S. K. Wexler, K. M. Hiscock and P. F. Dennis, "Catchment-Scale Quantification of Hyporheic Denitrification Using an Isotopic and Solute Flux Approach," *Environmental Science & Technology,* vol. 45, no. 9, pp. 3967-3973, 2011.

[40] C. Kendall, "Chapter 16: Tracing Nitrogen Sources and Cycles in Catchments," in *Isotope Tracers in Catchment Hydrology*, Amsterdam, Elsevier, 1998.

[41] Bottcher, et al., "Using Isotope Fractionation of Nitrate-Nitrogen and Nitrate-Oxygen for Evaluation of Microbial Denitridication in a Sandy Aquifer," *J. Hydrology,* vol. 114, pp. 413-424, 1990.

[42] K. Casciotti, D. M. Sigman, M. Galanter Hastings, J. K. Bohlke and A. Hikert, "Measurement of the Oxygen Isotopic Composition of Nitrate in Seawater and Freshwater Using the Denitrifier Method," *Analytical Chemistry,* vol. 74, pp. 4905-4912, 2002.

[43] D. Sigman, K. L. Casciotti, M. Andreani, C. Barford, M. Galanter and J. K. Bohlke, "A Bacterial Method for hte Nitrogen Isotopic Analysis of Nitrate in Seawater and Freshwater," *Analytic Chemistry,* vol. 73, pp. 4145-4153, 2001.

[44] EPA, "Clean Air Status and Trends Network (CASTNET)," [Online]. Available: http://epa.gov/castnet/javaweb/index.html.

[45] R. Rutting, P. Boeckx, C. Muller and L. Klemedtsson, "Assessment of the importance of dissimilatory nitrate reduction to ammonium for the terrestrial nitrogen cycle," *Biogeosciences,* vol. 8, pp. 1779-1791, 2011.

[46] J. Davis, S. M. Griffith, W. R. Horwath, J. J. Steiner and D. D. Myrold, "Denitrification and Nitrate Consumption in an Herbaceous Riparian Area and Perennial Ryegrass Seed Cropping System," *Soil Science Society of America Journal,* vol. 72, pp. 1299-1310, 2008.

[47] K. Hayhoe, C. P. Waker, T. G. Huntington, L. Luo, M. D. Schwartz, J. Sheffield, W. Wood, B. Anderson, J. Bradbury, A. DeGaetano, T. J. Troy and D. Wolfe, "Past and future changes in climate and hydrological indicators in the US Northeast," *Climate Dynamics,* pp. 381-407, 2007.

[48] R. Howarth, D. P. Swaney, E. W. Boyer, R. Marino, N. Jaworski and C. Goodale, "Influence of climate on average nitrogen export from large watersheds in the Northeastern United States," *Biogeochemistry,* pp. 163-186, 2006.

[49] H. Boyacioglu, T. Vetter, V. Krysanova and M. Rode, "Modeling the impacts of climate change on nitrogen retention in a 4th order stream," *Climate Change,* vol. 113, pp. 981-999, 2012.

[50] K. Butterbach-Bahl and M. Dannenmann, "Denitrification and associated soil N2O emisssions due to agricultural activities in a changing climate," *Current Opinion in environmental Sustainability,* pp. 389-395, 2011.

[51] NCDC, "National Climate Data Center," [Online]. Available: http://www.ncdc.noaa.gov/cdo-web/datasets/GHCND/stations/GHCND:USC00304174/detail. [Accessed 18 04 2013].

[52] Intergovernmental Panel on Climate Change (IPCC), "Working Group I: The Scientific Basis," [Online]. Available: http://www.ipcc.ch/ipccreports/tar/wg1/029.htm. [Accessed 15 05 2013].

[53] K. A. Hayhoe, "A Standardized Framework for Evaluating the Skill of Regional Climate Downscaling Techniques," *(Doctoral Dissertation),* 2010.

[54] L. E. Hay, R. L. Wilby and G. H. Leavesley, "A comparison of Delta Change and Downscaled GCM Scenarios for Three Mountainous Basins in the United States," *Journal of the American Water Resources Association,* vol. 36, pp. 387-397, 2000.

[55] P. H. Gleick, "Methods for evaluating the regional hydrologic impacts of global climatic changes," *Journal of Hydrology,* vol. 88, pp. 97-116, 1986.

[56] M. A. Altabet, R. Francois, D. W. Murray and W. L. Prell, "Climate-related variations in denitrification in the Arabian Sea from sediment 15N /14N ratios," *Nature,* vol. 373, pp. 506-509, 1995.

[57] K. Hayhoe, C. Wake, B. Anderson, X.-Z. Liang, E. Maurer, J. Zhu, J. Bradbury, A. DeGaetano, A. M. Stoner and D. Wuebbles, "Regional climate change projections for the Northeast USA," *Mitigation and Adaptation Strategies for Global Change,* pp. 425-436, 2008.